METALLURGICAL EVALUATION OF DOT-E7042-3000 CYLINDER D-99604

Prepared for:

U.S. Department of Transportation
400 Seventh Street S.W.
Washington D.C. 20590

Prepared by:

Timothy R. Smith, Ph.D., P.E.
310 Montgomery Street
Alexandria, VA 22314

08/27/98

Reference No.: 957-1943
Project No.: DC18129.000
QA ID No.: DC18129.000/AOFO/0898/TS05

Ex

TABLE OF CONTENTS

LIST OF FIGURES

1.0 Introduction

The U.S. Department of Transportation (DOT) contracted with Exponent Failure Analysis Associates (FaAA) to perform a metallurgical examination of the remains of a failed aluminum SCUBA cylinder. The cylinder is a DOT-E7042-3000 type[1] with serial number D99604 manufactured by Walter Kidde. The cylinder was seized by the U.S. DOT on February 4, 1998 in Riviera Beach, Fl.

The scope of this investigation was to perform a detailed evaluation of the cylinder remains, including photodocumentation and non-destructive examinations, chemical and mechanical property determination, metallographic sectioning, and fractography. The detailed work scope for this evaluation is provided in Appendix A. This report presents the findings of this evaluation.

2.0 Visual Examination

A visual examination of the cylinder remains was performed. The remains are shown in Figures 1 and 2, in the as-received condition. The cylinder broke apart into four pieces, designated 1A, 2A, 3A and 4A by FaAA.

The E7042 exemption stampings on the neck of the aluminum cylinder indicate that it was manufactured by Walter Kidde. Further stampings on the neck indicated that the first hydrostatic test on it was performed in 09/79. This is taken as its date of manufacture. Inspection stampings indicated that the cylinder had been pressure re-tested on 07/82, 09/87, 02/92 and 11/94 [2]. A complete photodocumentation of the pieces was undertaken and is presented in Appendix B.

The fracture surfaces of the cylinder present on each of the four fragments were inclined (i.e., non-radial with respect to the cylinder axis) shear-type, except in the neck region where the fracture surfaces were flat and radial with respect to the axis of the cylinder. The main fracture surface ran through essentially a full diameter of the inlet hole in the neck region. Figure 3 shows a photomontage of the fracture surface in the neck region. Note the beach marks emanating from the inlet hole.

Fragment 2A, containing one-half of the neck region, sustained impact damage to its fracture surface and to its portion of the cylinder exterior, presumably all a result of the

[1] DOT E7042 is an exemption to the provisions of DOT's then-applicable Hazardous Materials Regulations granted to Walter Kidde to manufacture, mark and sell cylinders for the use in transportation in commerce of certain liquefied and nonliquefied compressed gases. This exemption satisfies the DOT-3Al section of 49 CFR-178.45.

[2] The 49 CFR 173.23(c) section dealing with Previously Authorized Packaging requires that cylinders manufactured under the E7042 exemption be stamped with the specification identification "3AL" before or at the next retest after July 2, 1982. This required stamping of the cylinder was not done.

rupture event. Other pieces also showed impact damage at certain locations and scuffmarks. These also all appeared to be from the rupture event.

In the neck region, the inside wall of the cylinder in this region shows multiple folds (or cusps) from the original manufacturing process (see Figure 3). The fracture surface on both sides of the inlet hole appears to pass through folds of this type. On fragment 2A, there were at least two cracks, labeled C1 and C2 on Figure 3, originating from these folds.

3.0 Quantitative Chemical Analysis

Samples of chips, taken using an electric drill from the neck, the sidewall, and the bottom of the cylinder, were dissolved in solution and analyzed by atomic absorption spectrometry to determine their chemical composition. The results of this analysis are shown in Table 1 and indicate that the cylinder conforms to the Aluminum Association (AA) 6351 alloy specification and satisfies the DOT-3AL specification for aluminum alloy chemistry.

Table 1: Chemistry of the Cylinder

	Composition (wt.%)				
Element	Test Result Neck	Test Result Side wall	Test Result Bottom	49 CFR-178.46-5 Specification (low)	49 CFR-178.46-5 Specification (high)
Mg	**0.66**	**0.66**	**0.64**	**0.40**	**0.80**
Si	**1.00**	**1.00**	**1.00**	**0.70**	**1.30**
Ti	**<0.02**	**<0.02**	**<0.02**	**0.00**	**0.20**
Mn	**0.52**	**0.53**	**0.52**	**0.40**	**0.80**
Fe	**0.15**	**0.16**	**0.15**	**0.00**	**0.50**
Cu	**0.02**	**<0.02**	**0.02**	**0.00**	**0.10**
Zn	**<0.02**	**<0.02**	**<0.02**	**0.00**	**0.20**
Bi	**<0.005**	**<0.005**	**<0.005**	**0.00**	**0.01**
Pb	**<0.01**	**<0.01**	**<0.01**	**0.00**	**0.01**
Al	**balance**	**Balance**	**balance**	**balance**	**balance**

Chemical composition determined by atomic absorption spectrometry in accordance with the ASTM-E663 and ASTM-D3335 standards.

These results show compliance with the current DOT federal regulation 49 CFR 178.46-5, with no significant variations based on the sample location from within the cylinder. Note that the Pb levels found were below the detection threshold of 100 weight-ppm (13 atomic-ppm[3]) for the sample size provided for chemical testing. In addition, the Bi-levels were below 50 weight-ppm (6.5 atomic-ppm).

[3] calculated using the equation: atomic-ppm (Pb) = weight-ppm (Pb)*GMW(Al)/GMW(Pb); where GMW is the gram molecular weight of the element in parenthesis. The same equation was used for the bismuth level with Bi replacing Pb.

4.0 Mechanical Testing

4.1 Tensile Testing

Full thickness tensile test coupons from the cylinder wall, aligned along the cylinder axis, were tested at room temperature in accordance with ASTM B 557 and following the procedure given by 49 CFR 178.46-13[4]. Samples were machined from the segment marked "Mech" in Figure 5b. The results of these tests are shown in Table 2.

The average strength values found are well above the current 49 CFR 178.46-5 minimum specification and meet the elongation requirements. They compare well with values of 42.8 ksi yield strength, 49.3 ksi ultimate strength and 13% elongation (2 inch gauge length), published for AA6351 in T6 temper [1]. The DOT 3AL specification requires that the material be AA6351-T6.

Table 2: Mechanical Properties

Test	Yield (ksi)	UTS (ksi)	Elongation (%)	49 CFR 178.46-5 Yield (min.) (ksi)	49 CFR 178.46-5 UTS (min.) (ksi)	Elongation (%)
T-1	**48.9**	**52.5**	**13.7**	**37.0**	**42.0**	**14**
T-2	**48.1**	**52.1**	**14.1**	**37.0**	**42.0**	**14**
T-3	**47.0**	**51.3**	**14.5**	**37.0**	**42.0**	**14**
Average	**48.0**	**52.0**	**14.1**	**37.0**	**42.0**	**14**

Notes:
1. Tests were performed in accordance with the ASTM B 557 standard; gauge length was 2 inches.
2. Yield denotes the yield strength (0.2% offset), UTS denotes ultimate tensile strength.
3. Elongation values from the flat coupons tested here differ from the 49 CFR 178.46-5 values based on cylindrical specimens.

4.2 Hardness Testing

Rockwell hardness measurements were made on a slice removed from the tank sidewall area. A total of five measurements were taken using a Leco RT-370 Rockwell hardness tester with a 100-kg load; the results are shown in Table 3.

[4] The DOT 3AL specification requires tensile test specimens, representing a cylinder lot, to be taken in pairs oriented 180 degrees apart. In these tests, three specimens, taken adjacent to one another, were tested to preserve as much of the cylinder remains as possible. The balance of test protocol used, however, followed the procedure described in 49 CFR 178.46-13.

Table 3: Hardness Measurements

Component	Indent No.	Hardness (Rockwell B)	Average Hardness (Rockwell B)
	1	57.8	60.6 HRB
	2	60.3	
	3	61.1	
	4	62.0	
	5	61.6	

5.0 Sectioning and Metallography

Figure 4 shows the sections cut from cylinder fragment 2A. Sections of the fracture surface on both sides of the inlet hole were cut such that the flat-faced portion of the fracture surface was separated from the fragment. Two wafers were generated in this process.

Figure 6 shows the further sectioning performed on fragment 2A-1 from the neck region. A section (2A-1F) was sliced in the neck region and then polished and etched to reveal its microstructure, Figure 7. Note that the grain size is relatively small, compared to the thickness at the neck. Figure 8 shows a higher magnification view of the thread area from Figure 7, about 2/3 of the way down the inlet hole. Note that there is corrosion pitting damage to the threads in this region.

The crack C1 at the inlet hole from Figure 3 was selected for further study. The crack was sectioned just below the inlet hole threads (Section 2A-1C) and then polished to reveal its morphology. Figure 9 shows the portion of the inlet hole threads that was separated in the sectioning process. Note that the crack C1 (marked "crack") and also several corrosion pits are shown. Figure 10 shows energy dispersive spectra (EDS) taken from at or near the corrosion pits shown in Figure 9. Note the O, Ca, Cl, Fe, and Cu peaks, all of which are corrosion product or contaminants. The Cu and Fe are most probably from the threaded end of the regulator assembly that was screwed into the inlet hole during service.

Figure 11 shows section 2A-1C containing crack C1 taken parallel to the inlet hole, just below the wafer shown in Figure 9. Note the multiple folds at the inside surface and multiple branched cracks emanating from these folds. Figure 11(a) shows the section after preparation with a $HF+H_2SO_4+H_2O$ etch. The microstructure is typical for AA6351 in the T6 temper condition [2]. Figure 11b-d show higher magnification view of the crack in Region A in Figure 11a. Note that the cracks show fine-scale branches. Figure 11e-f shows the cracks from Region B on Figure 11a. This region corresponds to the corrosion pitting noted in Figure 9 and is at a similar depth down the inlet hole to those shown in Figure 8. Note also that the crack appears to be discontinuous.

6.0 Fractography

The wafer containing the flat-faced fracture surface shown on the right in Figure 3 (section 2A-1A) was examined optically and in the scanning electron microscope (SEM). The optical examination revealed that the flat-faced region of the fracture surface shows little macroscopic ductility. Just outside of this region, the fracture surface transitioned to an inclined shear-type of fracture. The region just below the inlet hole threads and close to the inside of the cylinder contained some of the coating used to line the cylinder, suggesting that a deep fold was present at this location at the time of manufacture.

Fractography of the wafer also shows several beach marks (see Figure 3) in the flat-faced region, indicating progressive crack growth. Figure 12 shows a series of SEM fractographs taken from this fracture surface. Regions A-F are all flat-faced.

Region A (Figure 12a) was from near the inside of the tank, close to the threads at the inlet hole. Region B was close to Region A and contained a surface scale (Figure 12b) that obscured the fractographic details. Higher magnification views of Region C are shown in Figure 12c-d. This region contains predominantly intergranular fracture, with very fine-scale dimples on the faceted surfaces. In Regions D, E and F (Figures 12e-j), the fracture surface contains intergranular facets with very fine-scale poorly-formed dimples, but also contains progressively larger-scaled dimples at the locations further away from the inlet hole. Region G (Figure 12k-l) is in the shear-lipped region outside of the flat-faced portion of the fracture. This region shows predominantly dimpled rupture.

Figure 13 shows energy dispersive spectra (EDS) taken from the fracture surface of Figure 12. Figure 12a shows the spectrum for the region "A" which appears to be a coating of some sort. The spectrum shows Al and a small O peak, indicating that the coating is Al-based, perhaps formed by anodizing of the cylinder interior. Figure 13b shows the spectrum from the deposits found in Region "B", Figure 12b. The Cl, Si and O peaks indicate corrosion product or contaminants.

Section 2A-1B,containing the flat-faced fracture surface shown on the left in Figure 3, was also examined optically and in the SEM. As with Section 2A-1A, the flat-faced region of the fracture surface shows little macroscopic ductility and just outside of this region, transitions to an inclined shear-type of fracture. Figure 14 shows the results of the fractographic examination of this section. Figure 14a is an optical micrograph showing beach marking, described earlier. A series of SEM fractographs were taken at locations A-F on the fracture surface and are shown in Figure 14b-m. Regions A-E all show a predominantly intergranular fracture, with very fine-scale poorly formed dimples on the faceted surfaces. The fracture surface is all flat-faced in these regions and shows progressively larger-scaled dimples away from the inlet hole. Region F shows primarily ductile dimpled rupture and some intergranular faceting, with microdimpling on these facets.

Figure 15 shows SEM fractographs of the fracture surface from one of the tensile specimens (Specimen T-3) used for mechanical property determination. Note that the fracture surface is primarily ductile dimpled rupture, with both macro and micro dimples, and some intergranular faceting, with microdimpling on these facets. This morphology is consistent with fractographic studies of similar Al alloys in tensile and toughness testing [3]. This morphology compares well with Figure 12k-l and 14l-m.

7.0 Discussion

Examination and testing of the cylinder remains demonstrates that the subject cylinder meets the chemical and mechanical property requirements of DOT 3AL specifications in the current DOT 49 CFR 178.46. Both lead (Pb) and bismuth (Bi) are below the regulation limits specified in 49 CFR 178.46-5. The cylinder alloy complies with the Aluminum Association specification for AA6351-T6 in accordance with DOT 3AL. The microstructure appears to be typical for this alloy and heat treatment.

Examination of the fracture surfaces of each cylinder fragment suggests that the failure originated from the neck region of the cylinder near to the inlet hole. The flat-faced (i.e., radial) nature of the fracture surface at the neck region with little macroscopic ductility followed by a transition to an inclined (i.e., non-radial) shear-type of fracture on both sides of the cylinder, suggests fast fracture, initiating nearly simultaneously on both diametrally opposed sides of the inlet hole prior to final rupture. It is clear from Figure 3 that a sub-critical crack of some size existed on each side of the inlet hole. Both of these sub-critical cracks grew and were incorporated into the fracture surface. It is not clear which of these two diametrally-opposed cracks reached critical size first since both are nearly the same size. Once one of these cracks reached critical size, its rapid growth would immediately supply moments and forces on the other crack tip to get it to propagate nearly simultaneously.

The shape and location of the beach marks on the fracture surface segments studied in detail (Figures 12 and 14) suggests that the cracks propagated sub-critically (i.e., slowly) for the majority of the flat-faced region. This continued up to the extent defined by the last beach mark on each side of the inlet hole. The morphology of the beach marking is asymmetric suggesting that the crack origins were not the same on each side. The fracture on the right side of Figure 3 (Section 2A-1A) propagated from an origin at the inside surface at the inlet hole and below the threads. The presence of the darkened region, similar in color to the inside of the cylinder, on the fracture surface shows that the origin of the crack was a fold in the inside cylinder wall. The fracture on the left side of Figure 3 (Section 2A-1B) appear to have originated in the lower half of the threads at the inlet hole. This region is the site of localized pitting corrosion damage (such as seen in Figures 7, 8 and 9). Apart from the initial origin, the cracks that developed on both sides of the inlet hole show very similar characteristics and appear to have grown by the same mechanism.

The beach marks shown on the fracture surface in the neck are consistent with the morphology of cracked regions at the neck of other DOT-6498, DOT-3Al, and DOT-7235 aluminum cylinders that were rejected during hydrostatic retesting [4] and with an Australian-specification aluminum cylinder that leaked during filling [5].

Sectioning of the cylinder wall just below the threads at the inlet hole revealed multiple cracks from multiple origins at folds (or cusps) in the inside wall. These branched cracks are consistent with cracks found in the neck region of other DOT-6498, DOT-3Al, and DOT-7235 aluminum cylinders [4]. Since no fatigue striations or evidence of stress-corrosion cracking (SCC) were found, the observed cracks are more consistent with studies of "sustained-load cracking" reported in the literature for similar Al alloys [3, 6-10] than a fatigue or SCC sub-critical crack growth mechanism.

8.0 Summary and Conclusions

A metallurgical examination of an aluminum cylinder DOT-E7042-3000 type, with serial number D-99604 showed the following results.

- This 1979-vintage cylinder meets the chemical requirements of the 3AL specification in 49 CFR 178.46-5 for AA6351 alloy, including lead (Pb) and bismuth (Bi) levels.
- This 1979-vintage cylinder meets the mechanical property requirements of the 3AL specification in the current 49 CFR 178.46-5.
- Multiple cracks were found originating at folds in the interior wall in the neck region near the inlet hole. These folds were associated with the cylinder's manufacture.
- Cracks showed a multiple-branched morphology; crack tips appeared to be discontinuous.
- The cylinder failed from the neck region when a sub-critical crack(s) in the neck region grew to critical size. The primary fracture surfaces developed from cracks at folds on the interior wall and pitting corrosion damage in the thread area of the neck.
- The apparent origin of the fracture is consistent with sustained-load cracks reported in the literature for similar Al alloys. The crack size at the time of rupture appears to be defined by the macroscopic beach marks on the flat-faced (i.e., radial) portions of the fracture surface that were furthest away from the inlet hole.

9.0 References

1. J. E. Hatch, Ed., (1984). Aluminum: Properties and Physical Metallurgy, American Society for Metals, Metals Park, OH, p. 363.

2. ASM Metals Handbook, 9th. Ed., Vol. 9, "Metallography and Microstructures", American Society for Metals, Metals Park, OH, p. 367.

3. M. Guttmann, B. Quantin, and Ph. Dumoulin (1983). "Intergranular creep embrittlement by non-soluble impurity: Pb precipitation hardened Al-Mg-Si alloys", Metal Sci., Vol. 17, No. 3, pp. 123-140.

4. J. H. Smith (1987). "Evaluation of Cracking in Aluminum Cylinders", NBSIR 86-3492, Institute for Materials Science and Engineering, National Bureau of Standards (NBS), U.S. Dept. of Commerce, Gaithersburg, MD.

5. J. W. H. Price, R. N. Ibrahim and D. Ischenko (1996). "Cracking in Aluminum 6061 and 6351 Gas Cylinders", Proc. Int. Conf. on Pressure Vessel Technology, Vol 1., American Society of Mechanical Engineers (ASME), Montreal, Canada, pp. 337-343.

6. J. J. Lewandowski, Y. S. Kim, and N. J. H. Holroyd (1992). "Lead-Induced Solid Metal Embrittlement of an Excess Silicon Al-Mg-Si Alloy at Temperatures of -4°C to 80° C", *Met. Trans. A.*, Vol. 23A, pp. 1679-1689.

7. Y. S. Kim, N. J. H. Holroyd, and J. J. Lewandowski (1989). "Pb-Induced Solid-Metal Embrittlement of Al-Mg-Si Alloy at Ambient Temperatures", *Proc. Environment-Induced Cracking of Metals*, National Association of Corrosion Engineers (NACE), pp. 371-377.

8. J. J. Lewandowski, V. Kohler, and N. J. H. Holroyd (1987). "Effects of Lead on the Sustained-load Cracking of Al-Mg-Si Alloys at Ambient Temperatures", *Mat. Sci & Eng.*, Vol. 96, pp. 185-195.

9. H. L. Stark and R. N. Ibrahim (1992). "Crack Propagation in Aluminum Gas Cylinder Neck Material at Constant Load and Room Temperature", Eng. Fracture Mechanics, Vol. 41, No. 4, pp. 569-575.

10. H. L. Stark and R. N. Ibrahim (1988). "Crack Propagation at Constant Load and Room Temperature in an Extruded Aluminum", Eng. Fracture Mechanics, Vol. 30, No. 3, pp. 409-414.

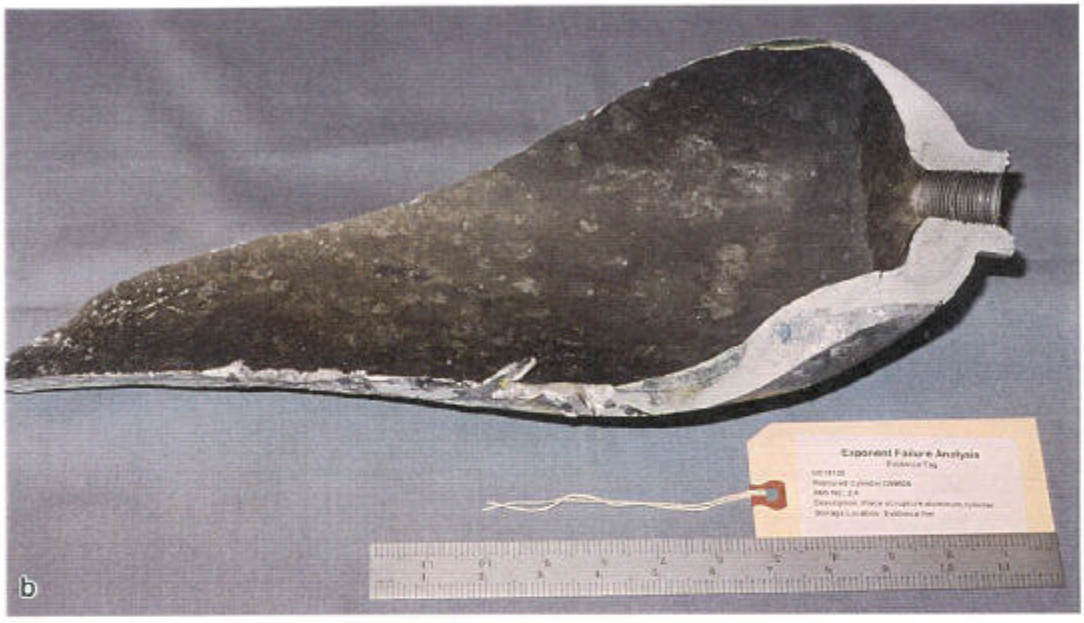

Figure 1: Cylinder remains, as received
(a) Fragment 1A. Photo ID: DC18129-R1E2.
(b) Fragment 2A. Photo ID: DC18129-R1E21.

Figure 2: Cylinder remains, as received
(a) Fragment 3A. Photo ID: DC18129-R2E21.
(b) Fragment 4A. Photo ID: DC18129-R3E11.

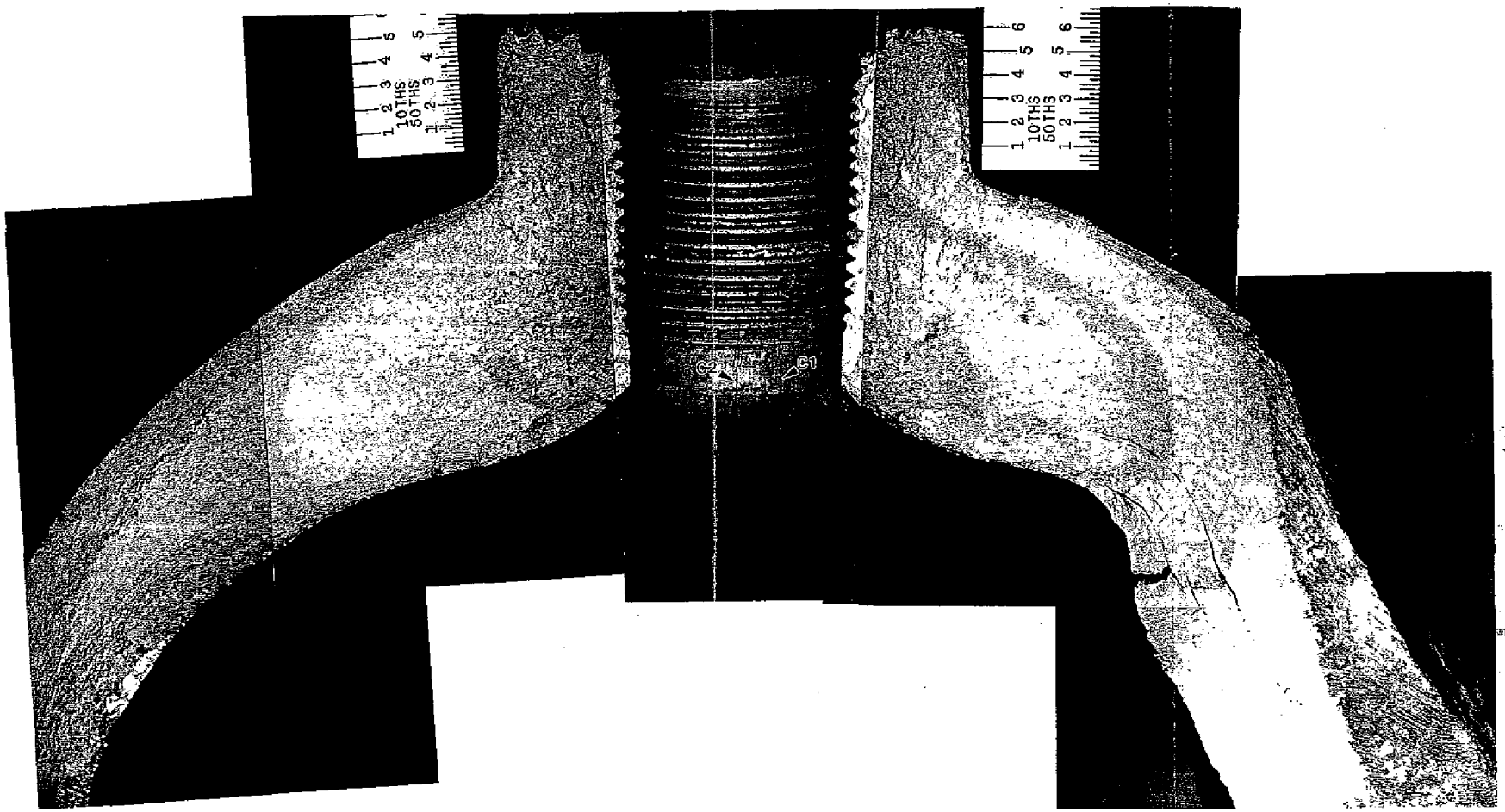

Figure 3. Photo montage of the fracture surface at the neck from fragment 2A. Photo ID: DC18129-R4E11,12,13,15,16.
Note the beach markings emanating from the inside diameter at the bottom of the inlet hole on one side and emanating from the threaded area of the inlet hole on the other. The pattern of these marks is asymmetric about the cylinder axis. Note also the cracks in the neck marked C1 and C2.

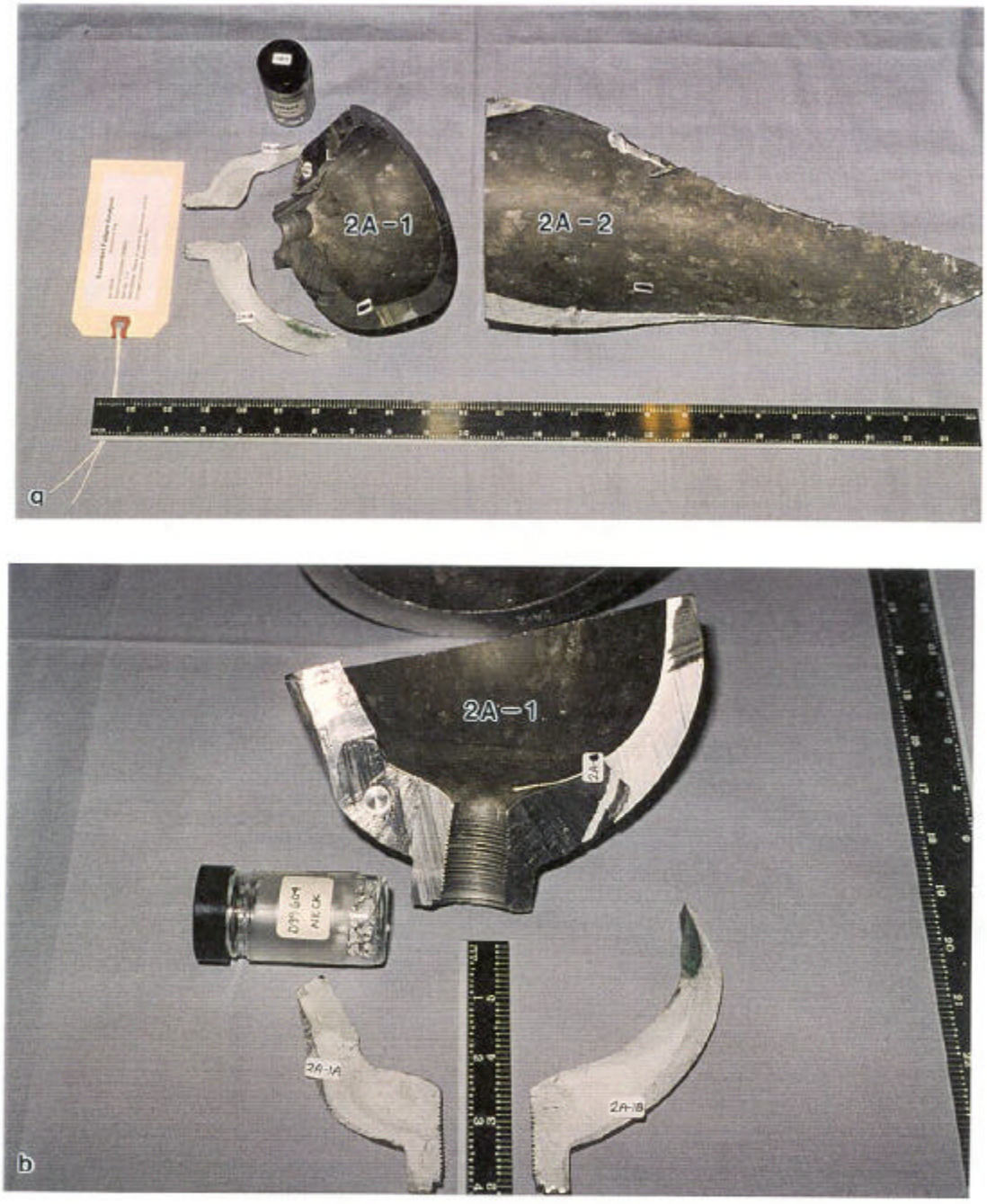

Figure 4. Sectioning of fragment 2A
(a) Overall view. Photo ID: DC18129-R3E4.
(b) Close up of neck region. Photo ID: DC18129-R3E8.
Note: the fracture surface portions that were removed and the drilling taken to determine chemical composition.

Figure 5. Sectioning of fragment 4A.
(a) Initial cuts showing the locations of drilling for chemical composition determination. Photo ID: DC18129-R3E16.
(b) Sectioning showing separated fracture surfaces and the portion used for tensile testing. Photo ID: DC18129-R5E3.

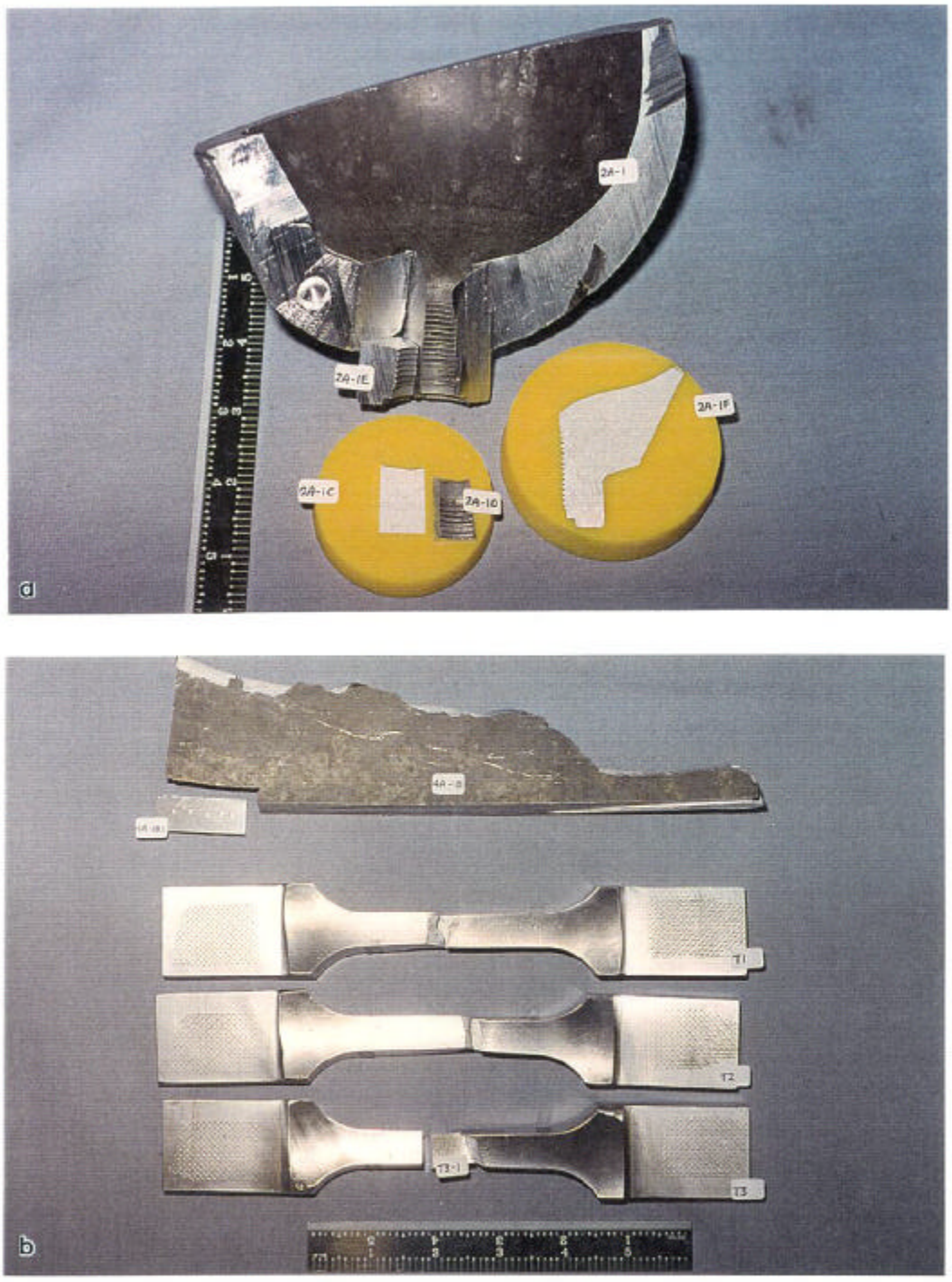

Figure 6. Additional sectioning of fragments 2A and 4A.
(a) Fragment 2A, neck region. Photo ID#: DC18129-R6E7.
(b) Fragment 4A, mechanical property samples.
Photo ID#: DC18129-R6E5.

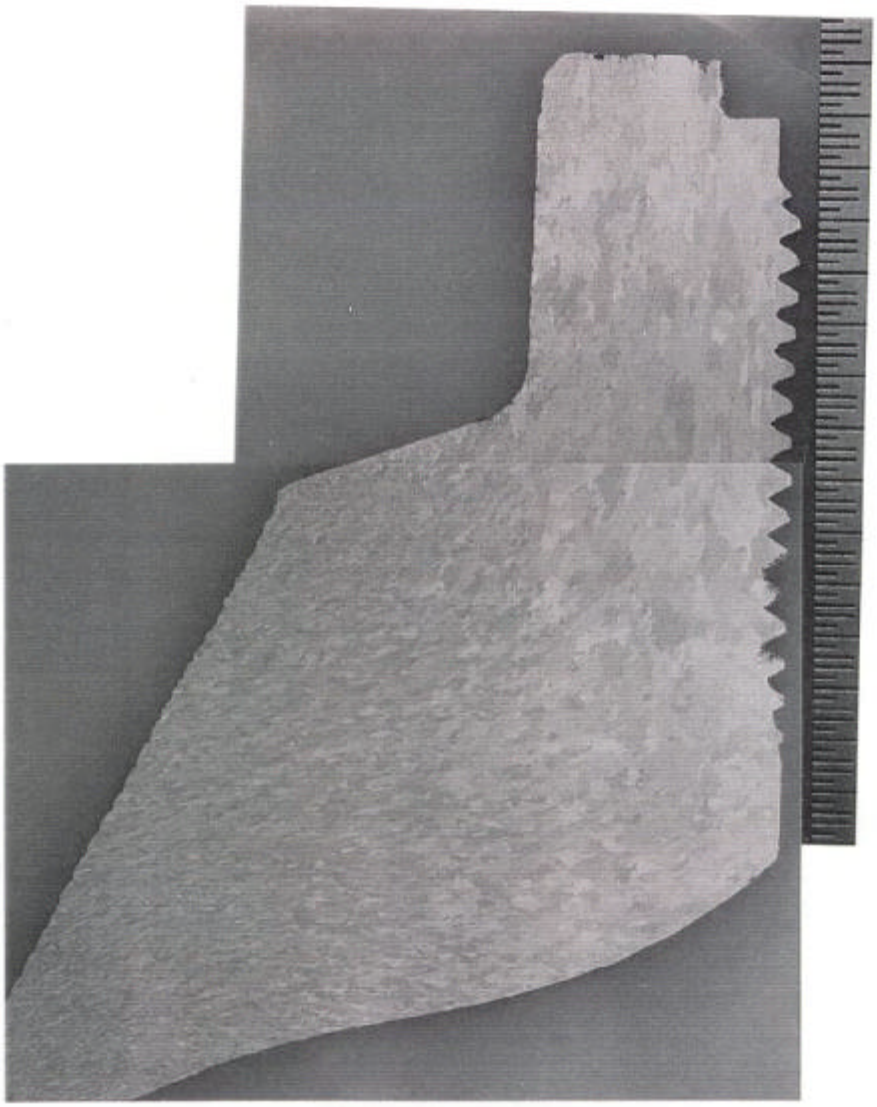

Figure 7. Section 2A-1F showing the microstructure in the neck region. Note the scale is in 0.05 inch increments. HF-H_2SO_4-H_2O etch. Photo ID: DC18129-PAL-1,2-7/28/98.

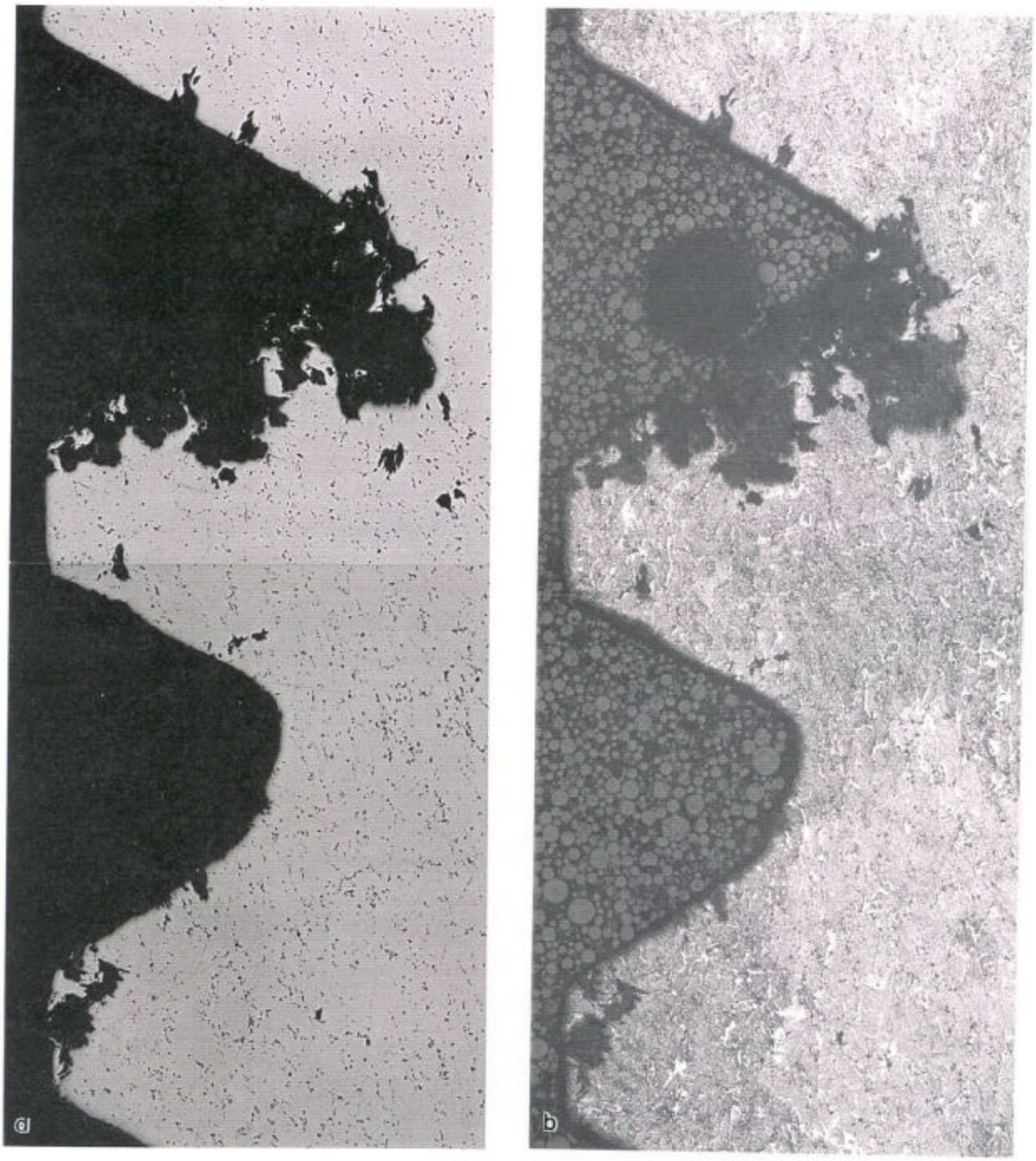

Figure 8. Close-up of thread area shown in Figure 7.
(a) 50X. Photo ID: DC18129-PAL-5,6-7/28/98.
(b) 50X. HF-H_2SO_4-H_2O etch. Photo ID: DC18129-PAL-9,10-7/28/98.
Note the corrosion pitting damage to the thread area.

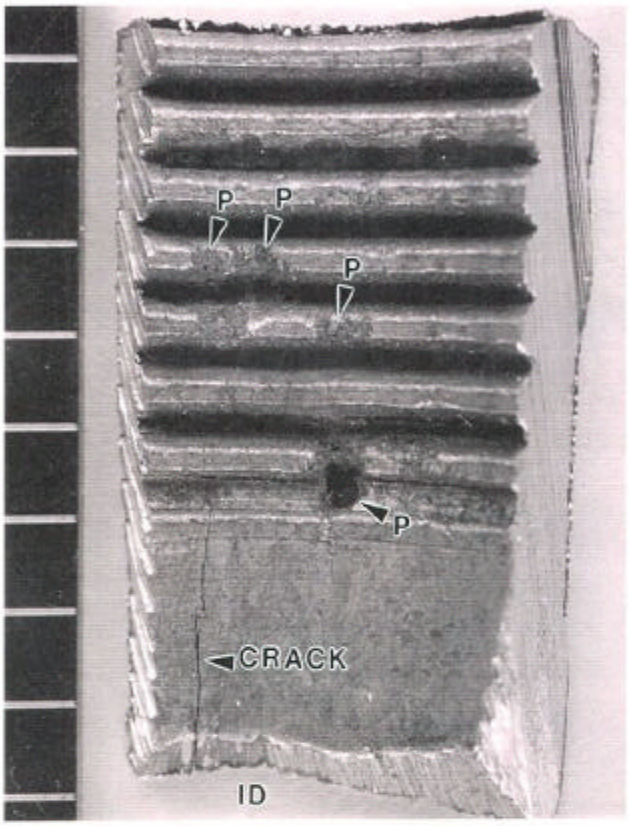

Figure 9. Close-up of portion of the inlet hole threads showing cracking and corrosion pits. Example pits are labeled "P". Scale is in 0.05 inch increments. Section 2A-1C was taken just behind this slice. Note that one pit forms a well-developed hole through this slice. Photo ID#: DC18129-TRS-1-8/5/98.

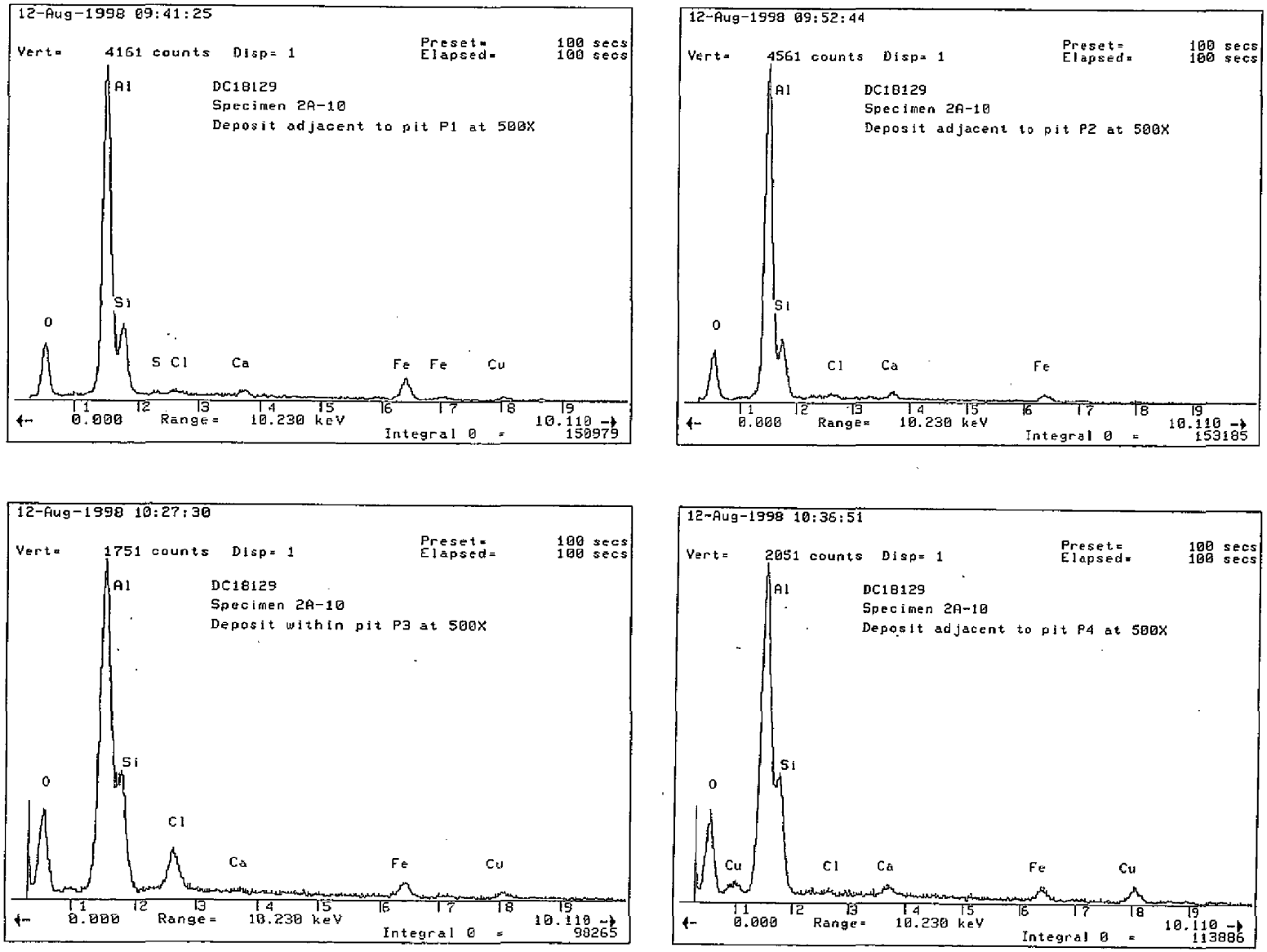

Figure 10. Energy dispersive spectra taken from at or near the pits shown in Figure 9.

Ex.

Figure 11. Section 2A-1C taken parallel to the inlet hole, just below the threads.

(a) Overall view of the section. HF-H_2SO_4-H_2O etch. Scale is in 0.05 inch increments. Note cracks in Regions A and B. Photo ID: DC18129-PAL-18-7/28/98.

(b) Close up of Region A. 50X. HF-H_2SO_4-H_2O etch. Note the folds on the surface. Photo ID: DC18129-PAL-18-7/28/98.

(c) Close up of Region A. 100X. Note the multiple branched cracks emanating from the folds on the surface. Photo ID: DC18129-PAL-21-7/28/98.

(d) Same as (c) in the etched condition. 100X. HF-H_2SO_4-H_2O etch. Photo ID: DC18129-PAL-22-7/28/98.

(e) Close up of Region B. 50X.. Photo ID: DC18129-PAL-28,29-7/28/98.

(f) Close up of Region B. 50X.. HF-H_2SO_4-H_2O etch. Photo ID: DC18129-PAL-30,31-7/28/98.

Note that due to instrument optics the micrographs 11b-f are mirror images of the corresponding regions in 11a.

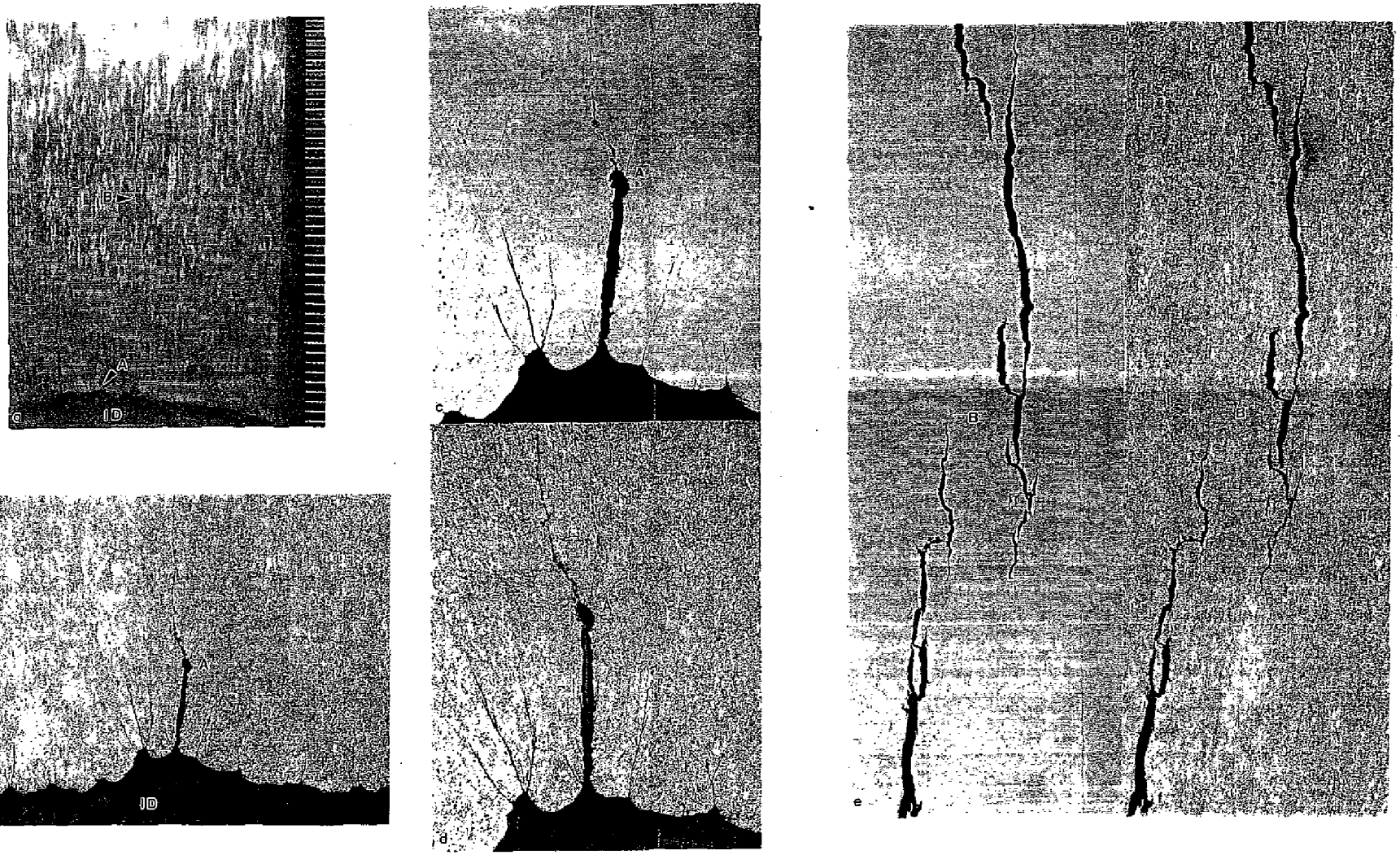

Figure 11.

Figure 12. Fractography of section 2A-1A. Overall optical micrograph view shows the regions examined in the SEM. Photo ID: DC18129-TRS-1-6/25/98.
(a) Region A showing the coating. 500X. Photo ID: DC18129-PAL-1-6/25/98.
(b) Region B showing deposits on the fracture surface. 500X. Photo ID: DC18129-PAL-3-6/25/98.
(c) Region C. 250X. Photo ID: DC18129-PAL-4-6/25/98.
(d) Region C. 1000X. Photo ID: DC18129-PAL-6-6/25/98.
(e) Region D. 250X. Photo ID: DC18129-PAL-8-6/25/98.
(f) Region D. 1000X. Photo ID: DC18129-PAL-11-6/25/98.
(g) Region E. 250X. Photo ID: DC18129-PAL-15-6/25/98.
(h) Region E. 1000X. Photo ID: DC18129-PAL-17-6/25/98.
(i) Region F. 250X. Photo ID: DC18129-PAL-19-6/25/98.
(j) Region F. 1000X. Photo ID: DC18129-PAL-21-6/25/98.
(k) Region G. 250X. Photo ID: DC18129-PAL-23-6/25/98.
(l) Region G. 1000X. Photo ID: DC18129-PAL-25-6/25/98.

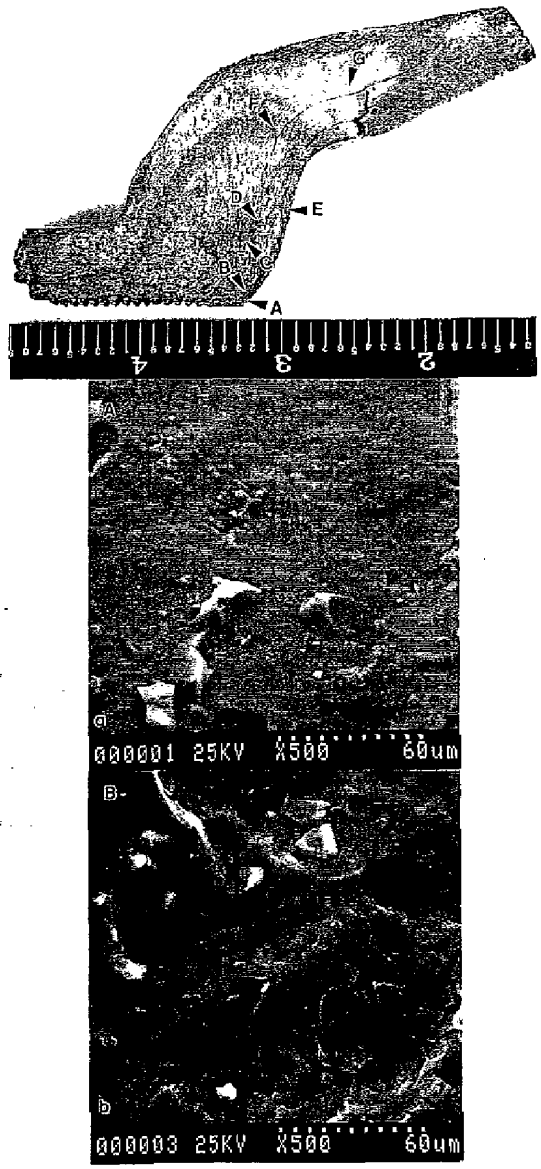
A
B
C
D
E
4
3
2
000001 25KV X500 60um
000003 25KV X500 60um

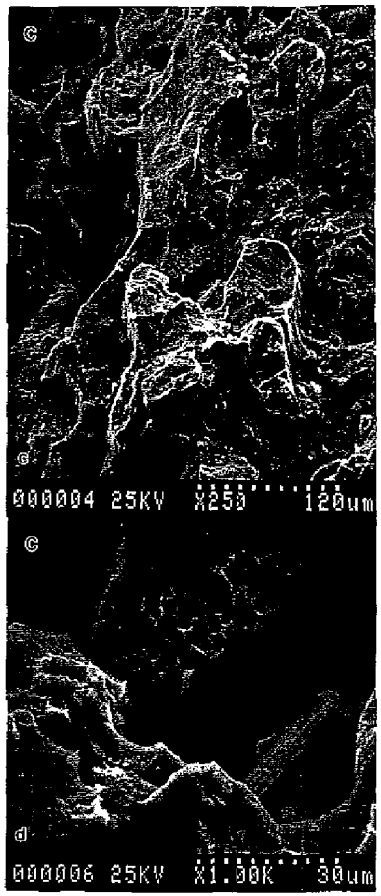
000004 25KV X250 120um
000006 25KV X1.50K 30um

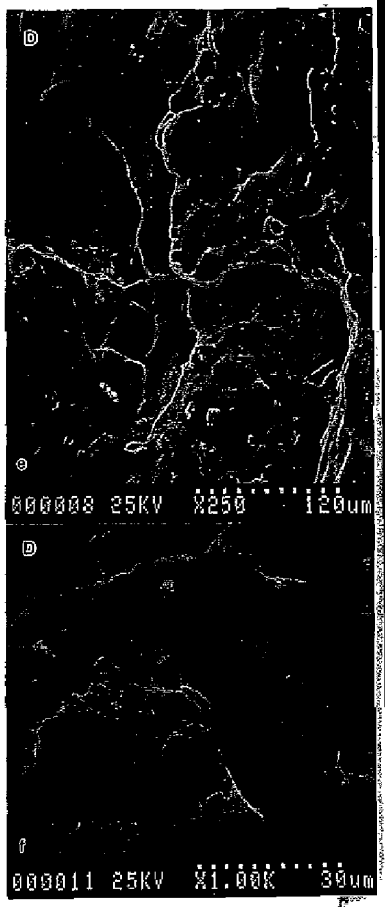
000008 25KV X250 120um
000011 25KV X1.00K 30um

Figure 12.

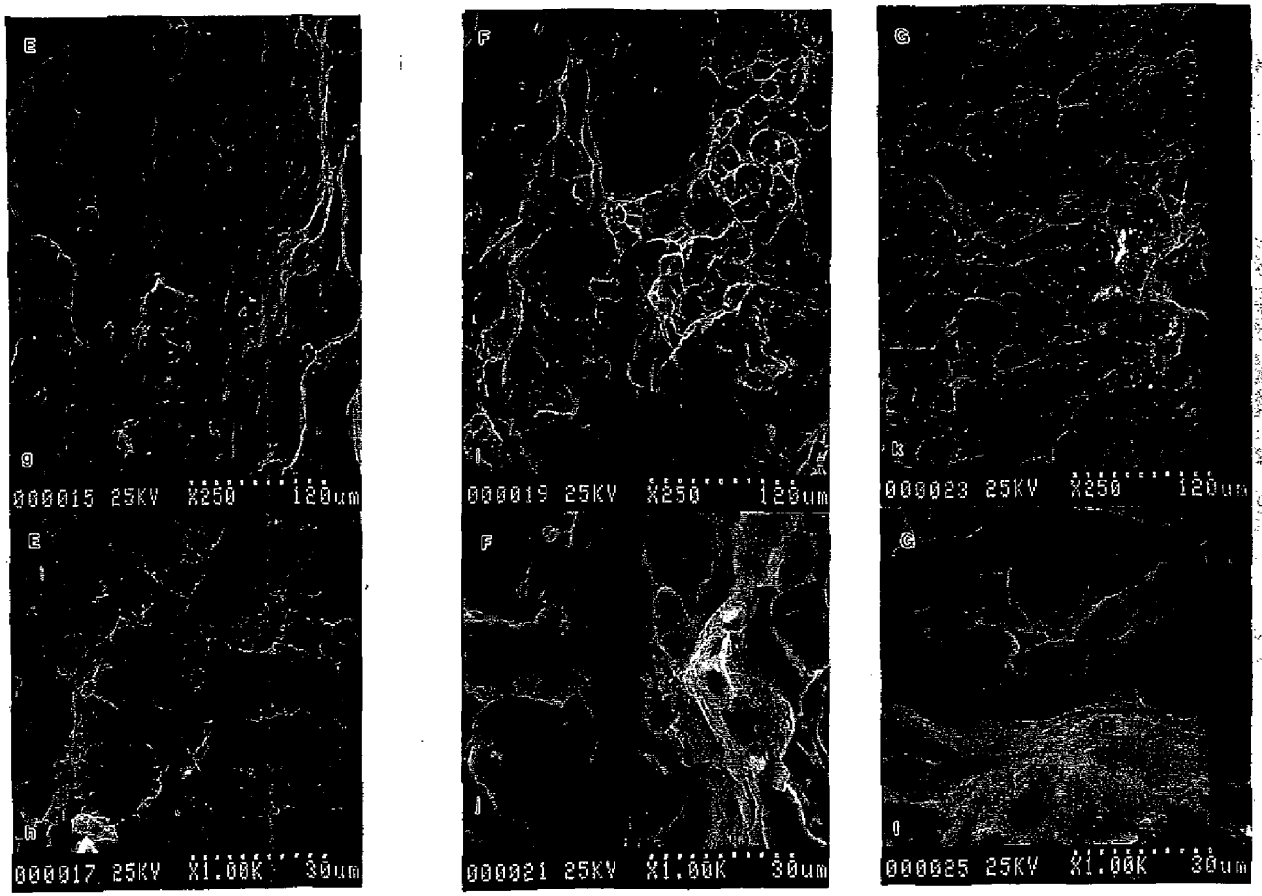
E
000015 25KV X250 120um
E
000017 25KV X1.00K 30um
F
000019 25KV X250 120um
F
000021 25KV X1.00K 30um
G
000023 25KV X250 120um
G
000025 25KV X1.00K 30um

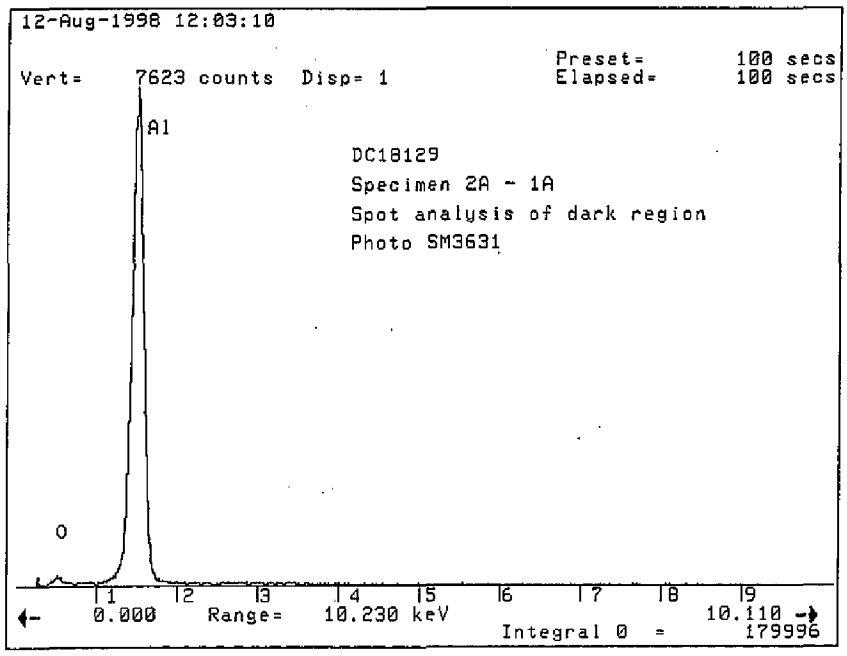

a

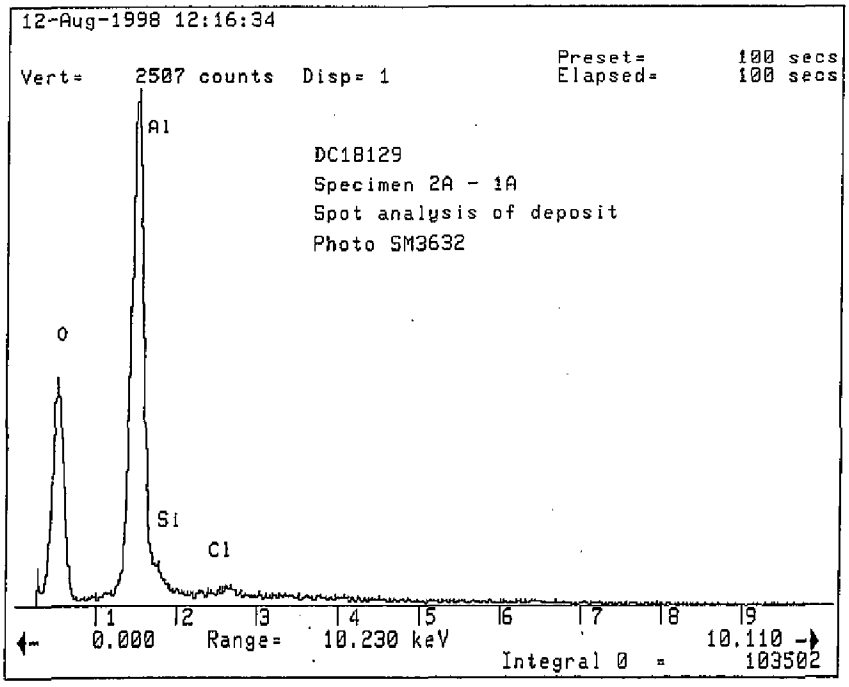

b

Figure 13. Energy dispersive spectra captured from the fracture surface of Figure 12.
(a) Spot analysis of coating region "A".
(b) Spot analysis of surface deposits from region "B"

Figure 14. Fractography of section 2A-1B. Photo ID: DC18129-TRS-1-6/25/98.
(a) Overall optical micrograph view shows the regions examined in the SEM. Scale is in 0.1 inch increments. Photo ID: DC18129-TRS-2-8/4/98.
(b) Region A. 250X.. Photo ID: DC18129-PAL-3-7/29/98
(c) Region A. 1000X. Photo ID: DC18129-PAL-4-7/29/98.
(d) Region B. 250X. Photo ID: DC18129-PAL-9-7/29/98.
(e) Region B. 1000X. Photo ID: DC18129-PAL-10-7/29/98.
(f) Region C. 250X. Photo ID: DC18129-PAL-5-7/29/98.
(g) Region C. 1000X. Photo ID: DC18129-PAL-6-7/29/98.
(h) Region D. 250X. Photo ID: DC18129-PAL-1-8/5/98.
(i) Region D. 1000X. Photo ID: DC18129-PAL-2-8/5/98.
(j) Region E. 250X. Photo ID: DC18129-PAL-3-8/5/98.
(k) Region E. 1000X. Photo ID: DC18129-PAL-4-8/5/98.
(l) Region F. 250X. Photo ID: DC18129-PAL-5-8/5/98.
(m) Region F. 1000X. Photo ID: DC18129-PAL-6-8/5/98.

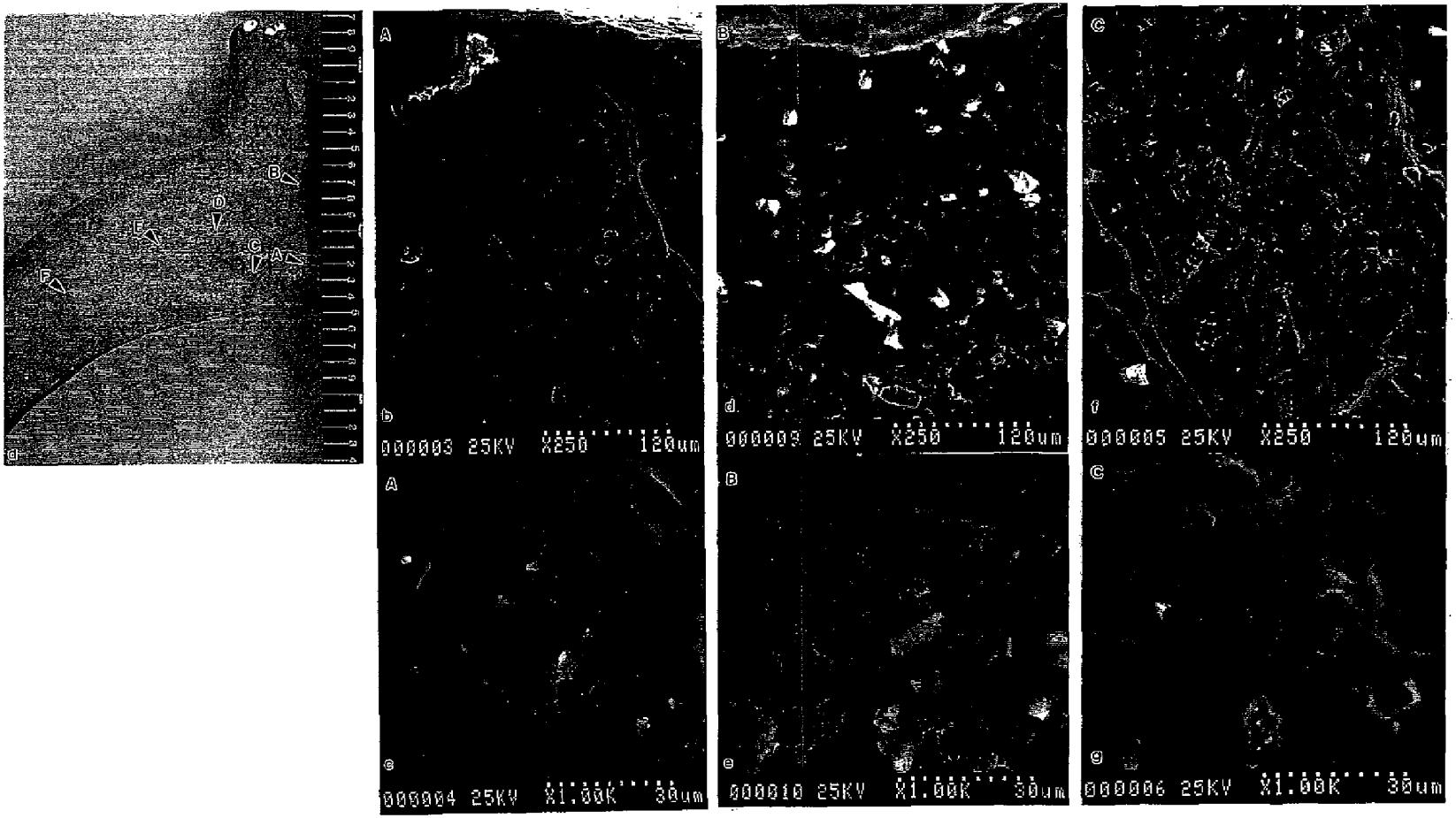
a
P
E
D
C
A
B
b
A
000003 25KV X250 120um
c
A
000004 25KV X1,00K 30um
d
B
000009 25KV X250 120um
e
B
000010 25KV X1.00K 30um
f
C
000005 25KV X250 120um
g
C
000006 25KV X1.00K 30um

Figure 14.

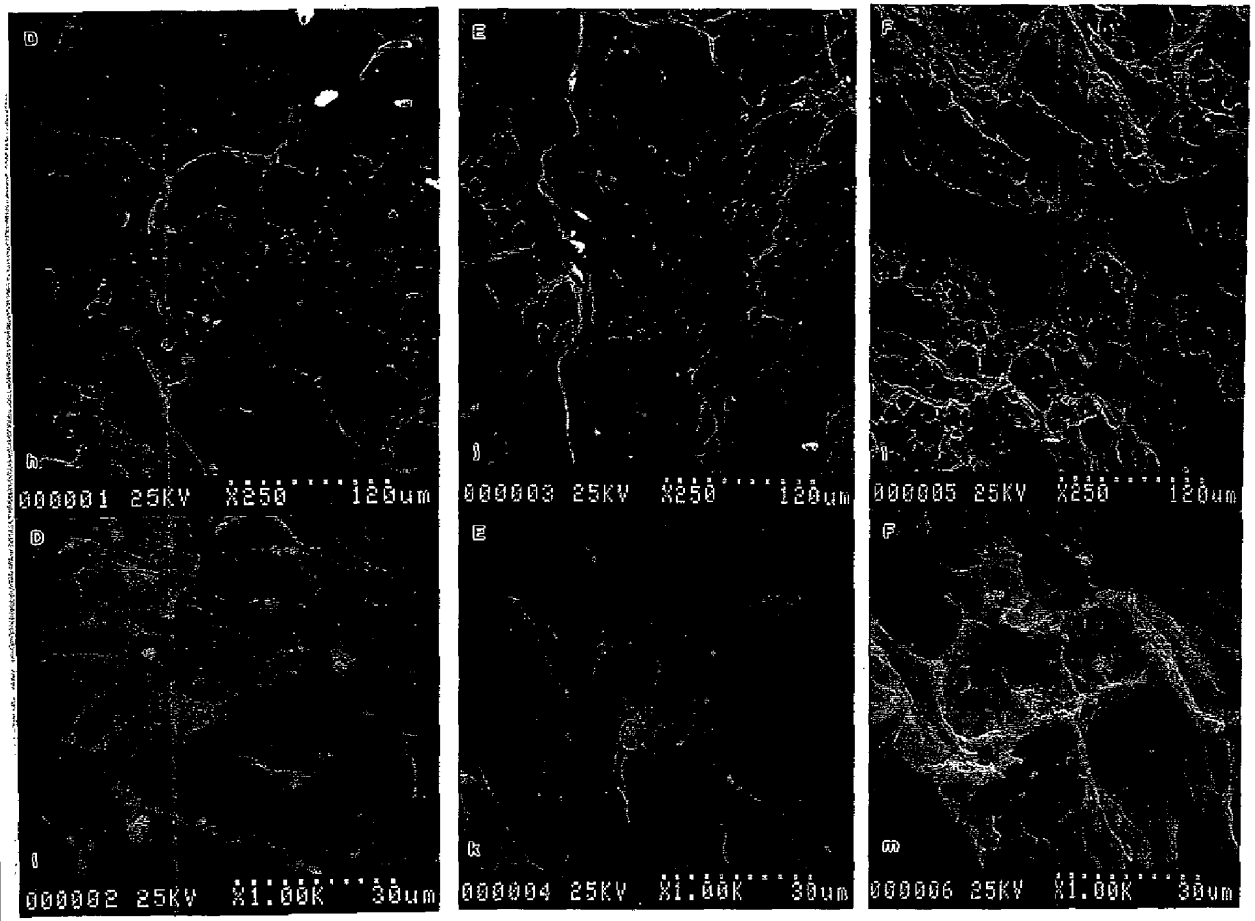
D
h
000001 25KV X250 120um
E
j
000003 25KV X250 120um
F
n
000005 25KV X250 120um
D
l
000002 25KV X1.00K 30um
E
k
000004 25KV X1.00K 30um
F
m
000006 25KV X1.00K 30um

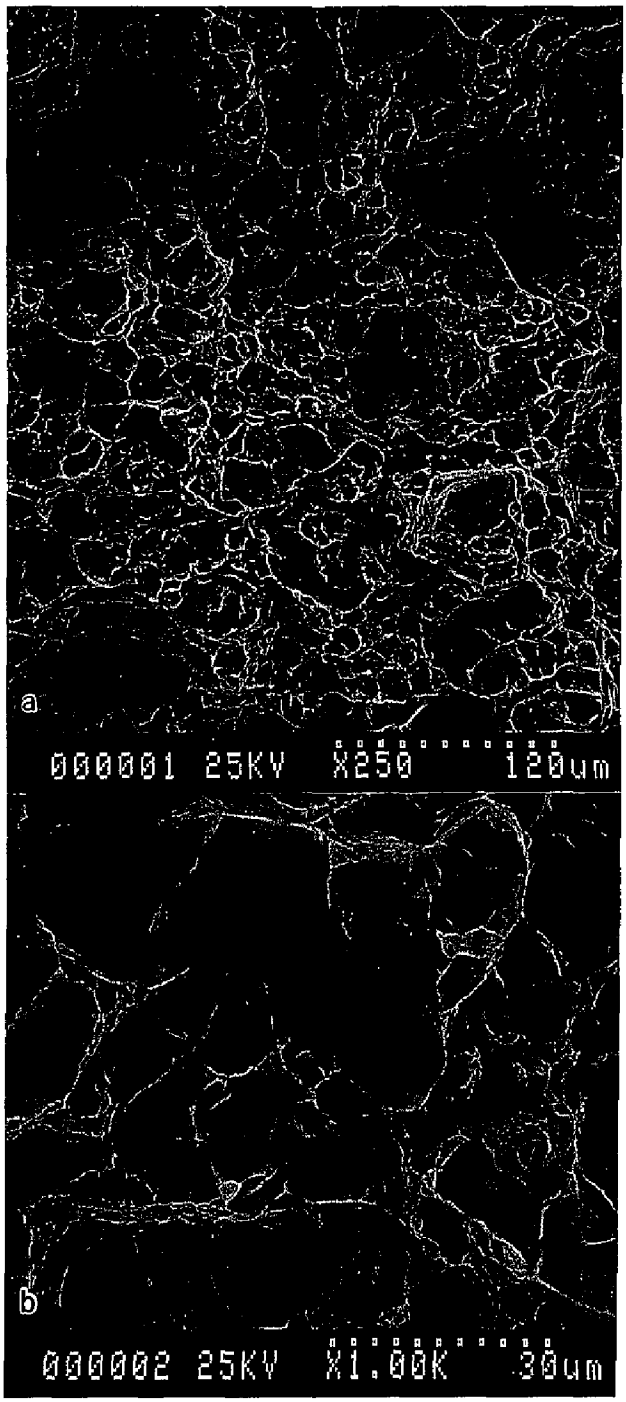

Figure 15. Fractography of tensile specimen T-3.
(a) 250 X. Photo ID: DC18129-PAL-1-8/4/98.
(b) 1000X. Photo ID: DC18129-PAL-2-8/4/98.

Appendix A: Recommended Scope of Work

Recommended Scope of Work for Metallurgical Evaluation of Aluminum Cylinder

1. Photodocumentation. Prior to any destructive examination of this cylinder, it will be photodocumented to illustrate its "as-received condition". After each cutting operation needed to remove samples for testing or evaluation (such as required for chemical samples) the cylinder and sample will be photodocumented to illustrate the sample location. Photodocument the primary fracture surface as well as any secondary cracks that may be present. Any corrosion deposits or other visible surface contaminates should also be photodocumented

2. Corrosion. Testing for corrosion product should be done prior to any extensive cutting or handling of the cylinder remains. Swipe samples or cutting of material containing any such potential corrosion products should be taken. When cutting is performed, care should be used to minimize contamination of the cylinder surfaces. Swipe samples or samples containing potential corrosion products should first be analyzed by scanning electron microscopy and energy dispersive spectroscopy (SEM/EDS).

3. Chemical Analysis. The cylinder aluminum alloy will be analyzed for chemical composition to compare with materials specifications. Material from the neck region, side wall and cylinder bottom will be analyzed to check for alloy homogeneity. The analysis will also determine the concentration of potentially detrimental trace elements, such as lead.

4. Macroetching. A thin slice of material will be removed from the neck of the cylinder that includes sidewall material. This slice will be macroetched to show the grain macro/microstructure in this area.

5. Fractography. SEM and stereo-microscopic examination should be performed on all fractures. Particular attention should be focused in the regions where the fracture originated. Any indications of fatigue, stress-corrosion cracking, ductile rupture, inter/intra-granular fracture features, etc., should be photodocumented.

6. Dimensional Checking. Prior to extensive cutting, the cylinder wall thickness at various locations and other cylinder features, such as threads, cylinder internal diameter, inlet hole diameter should be measured. Measurements done should be sufficient to determine the minimum wall thickness as well as to document any extensive plastic tearing that may have resulted in the failure event.

7. Secondary Cracking. A section of the primary fracture surface near the crack origin should be metallographically polished. Any secondary cracking near the failure origin should be evaluated. These sections should be first examined in the unetched condition and photodocumented to look for crack branching. The sample should then be etched, re-examined and photodocumented.

8. Material Hardness. The material hardness shall be evaluated in the neck, wall and cylinder bottom by means of macrohardness testing according to ASTM standards.

9. Physical Testing.

- mechanical test per 49 CFR, 178.46-13

10. Report. Report should contain a description of all tests performed and the results obtained. If possible, state the location of the crack origin, mode of fracture, and likely cause of failure.

Appendix B: Detailed Photodocumentation of Cylinder

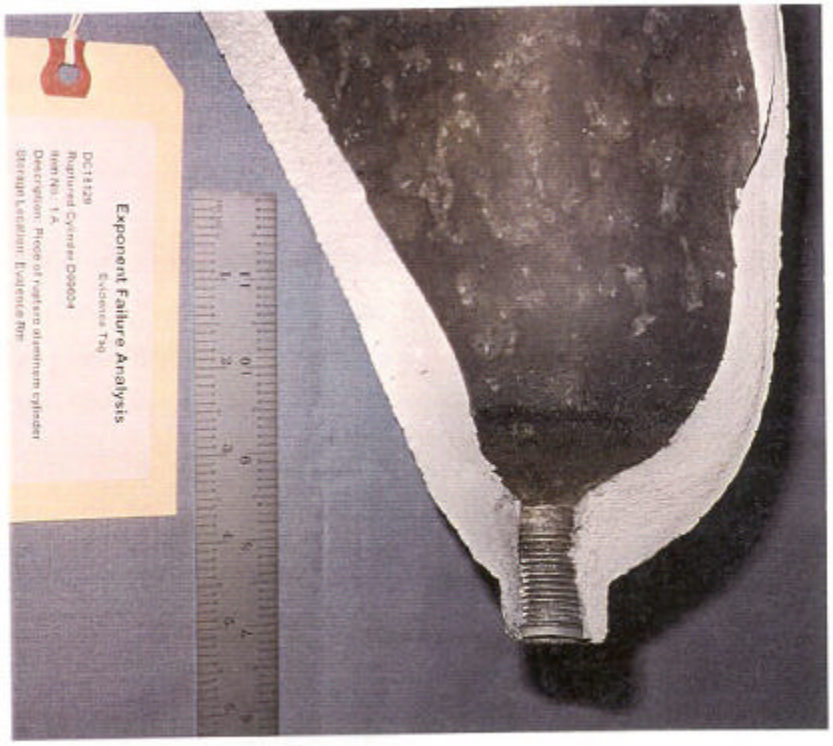

Photo ID: DC18129-R1E3

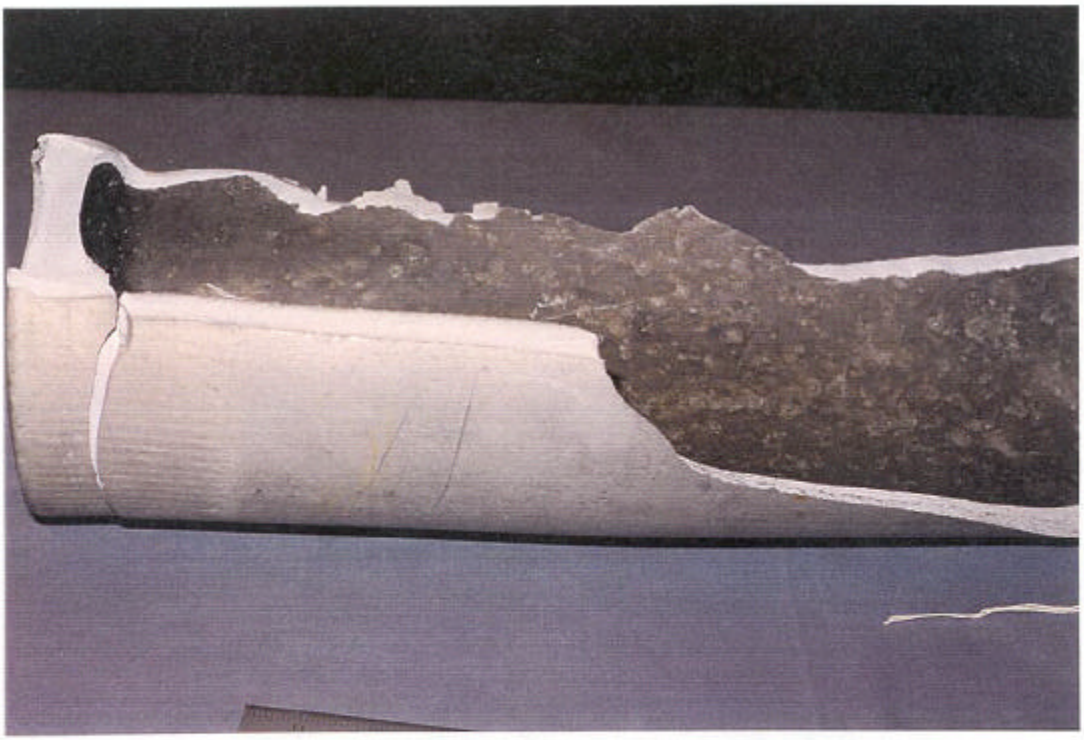

Photo ID: DC18129-R1E6

Ex.

Photo ID: DC18129-R1E4

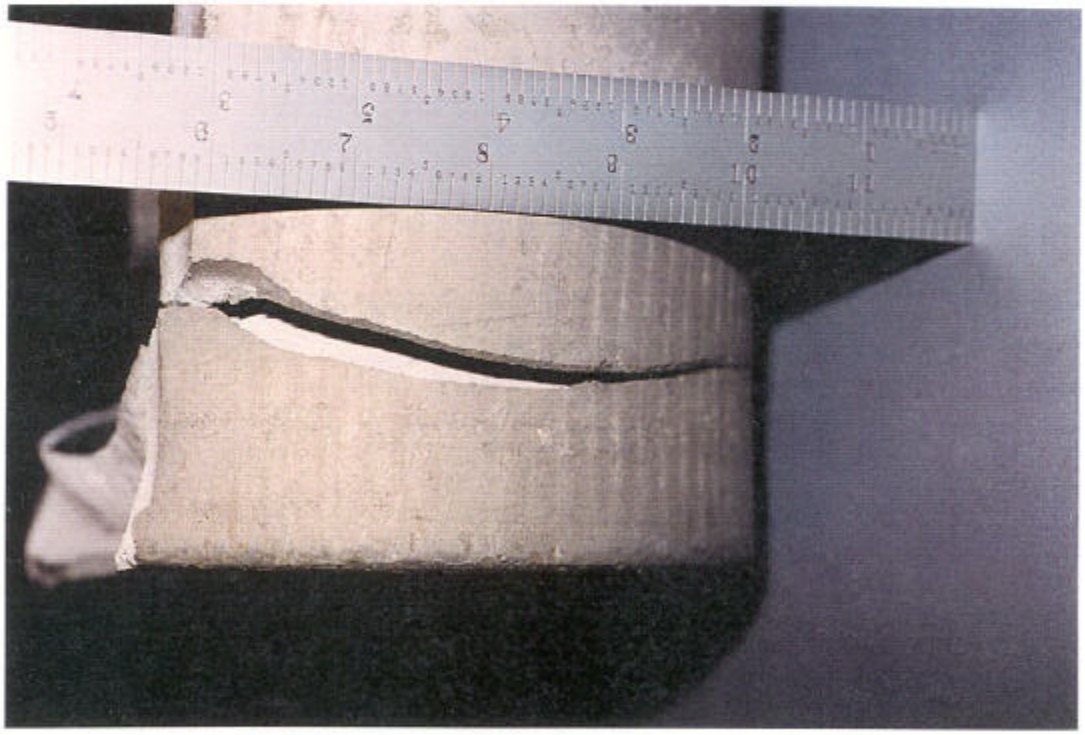

Photo ID: DC18129-R1E5

Ex.

Photo ID: DC18129-R1E8

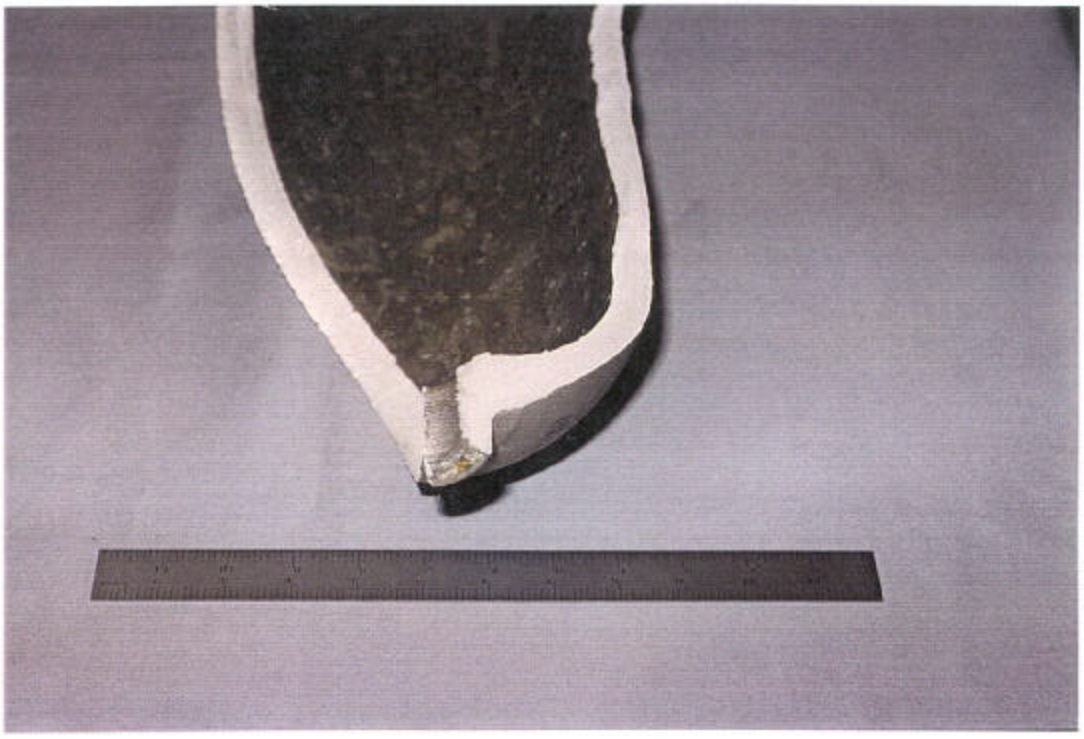

Photo ID: DC18129-R1E10

Ex.

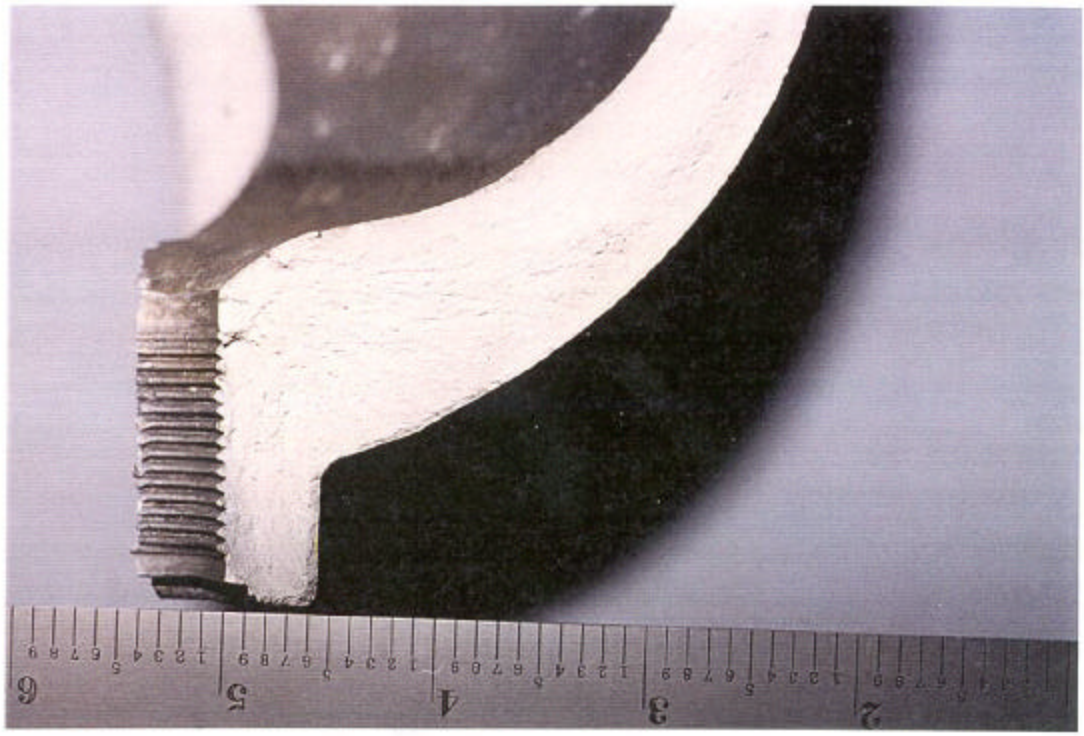

Photo ID: DC18129-R1E11

Photo ID: DC18129-R1E12

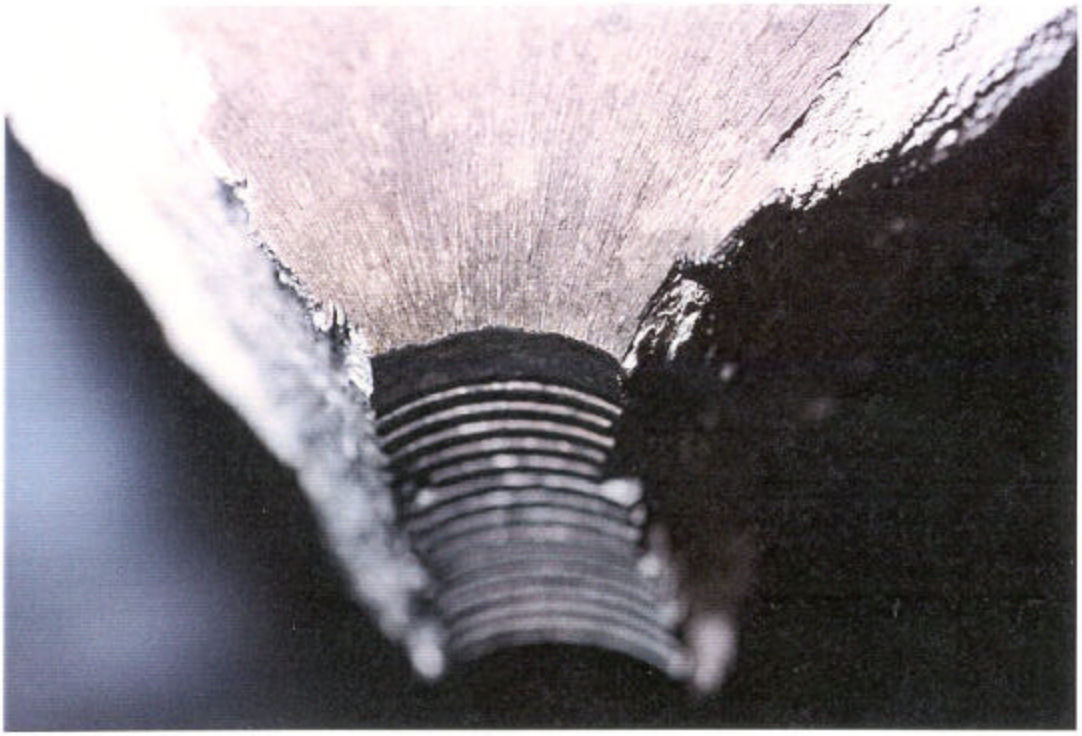

Photo ID: DC18129-R1E19

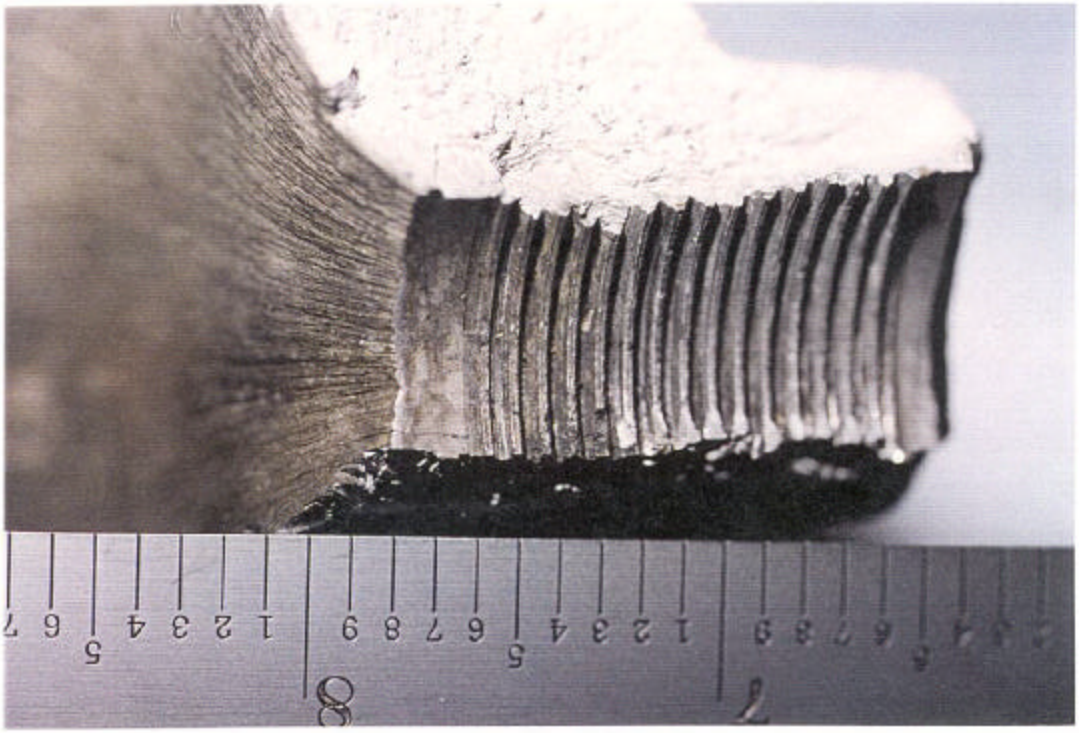

Photo ID: DC18129-R1E20

Photo ID: DC18129-R1E13

Photo ID: DC18129-R1E14

Ex.

Photo ID: DC18129-R1E15

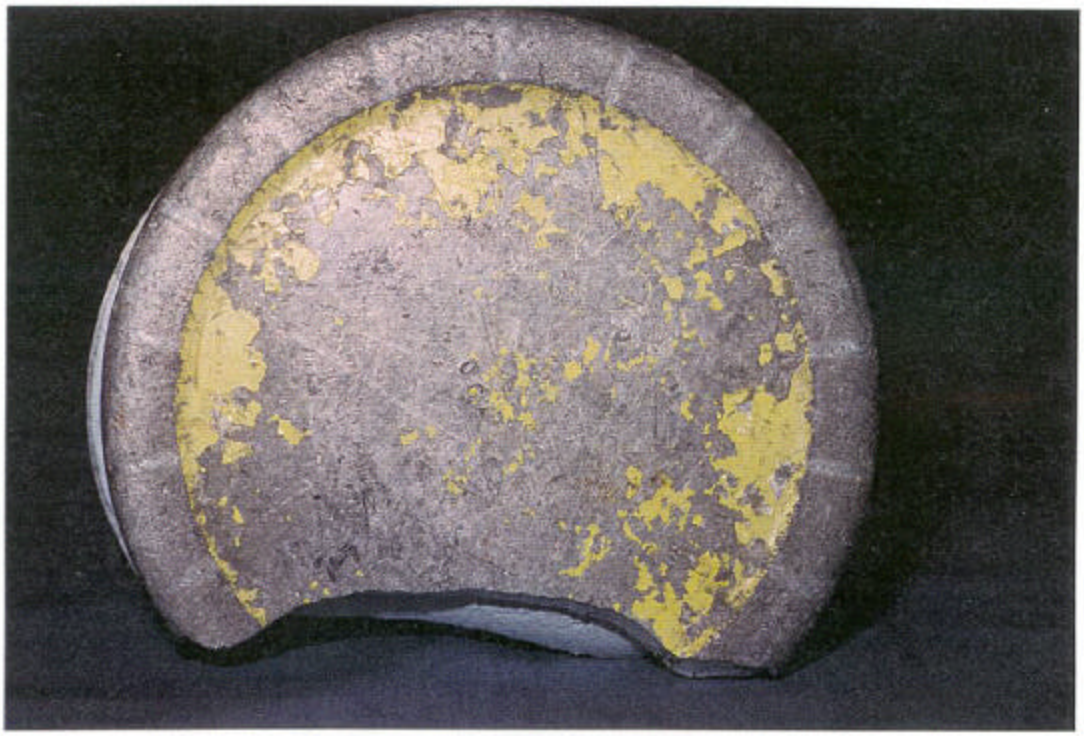

Photo ID: DC18129-R1E16

Ex.

Photo ID: DC18129-R1E17

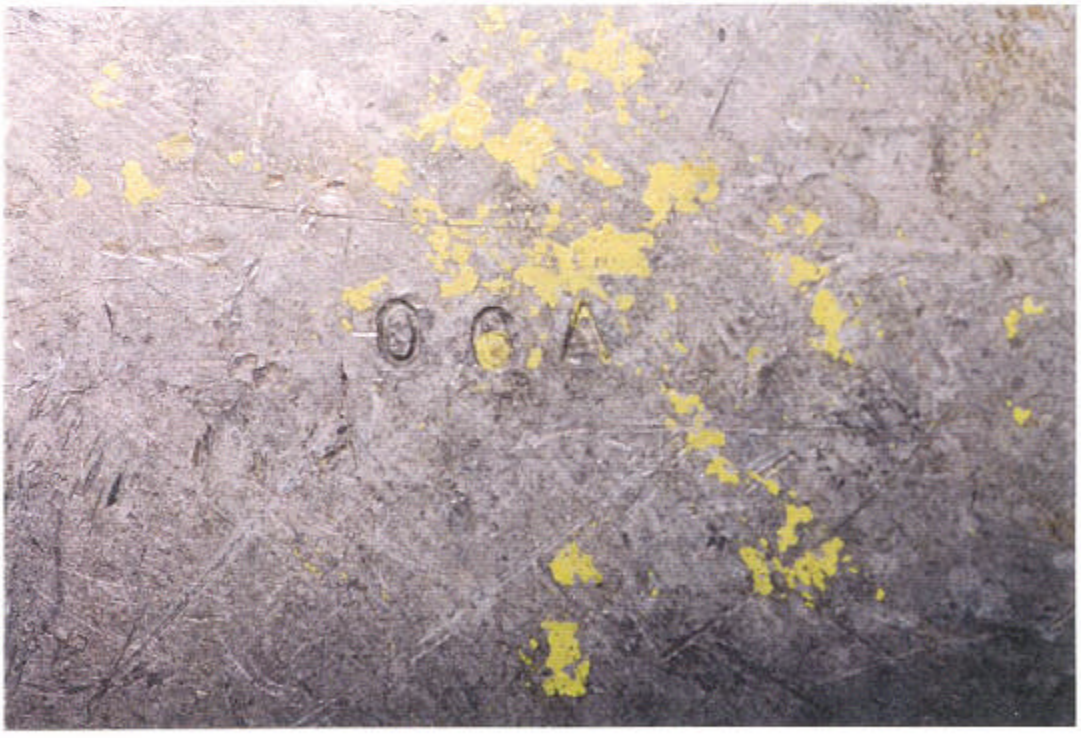

Photo ID: DC18129-R1E18

Ex.

Photo ID: DC18129-R2E3

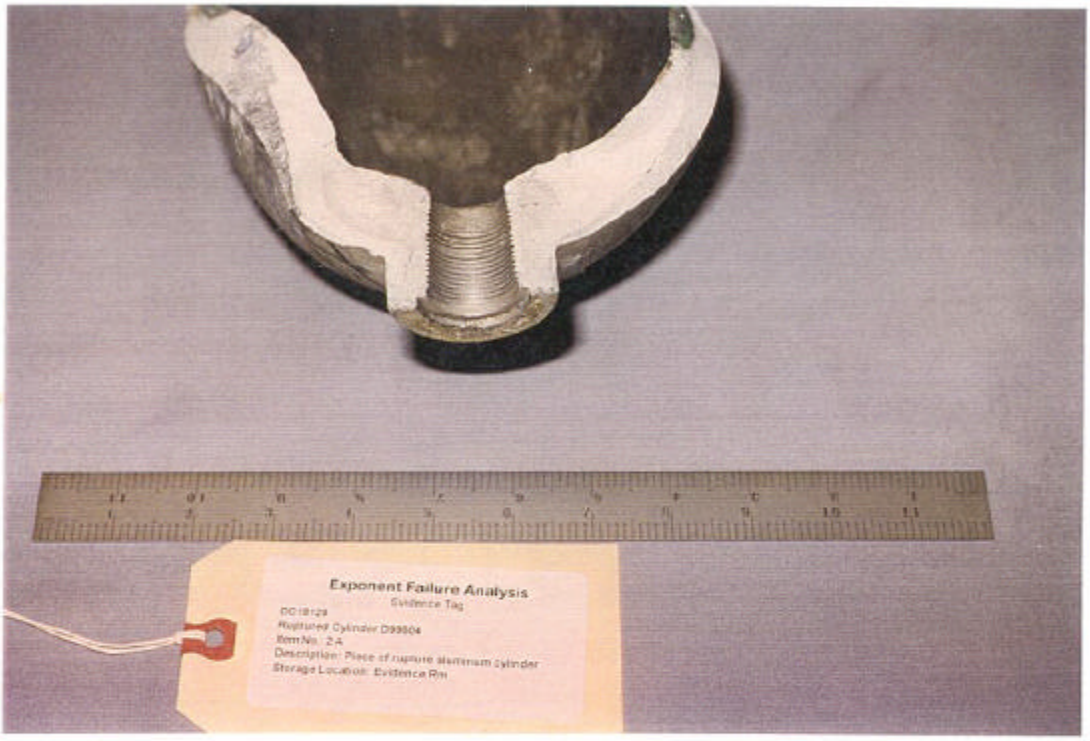

Photo ID: DC18129-R2E5

Ex.

Photo ID: DC18129-R1E22

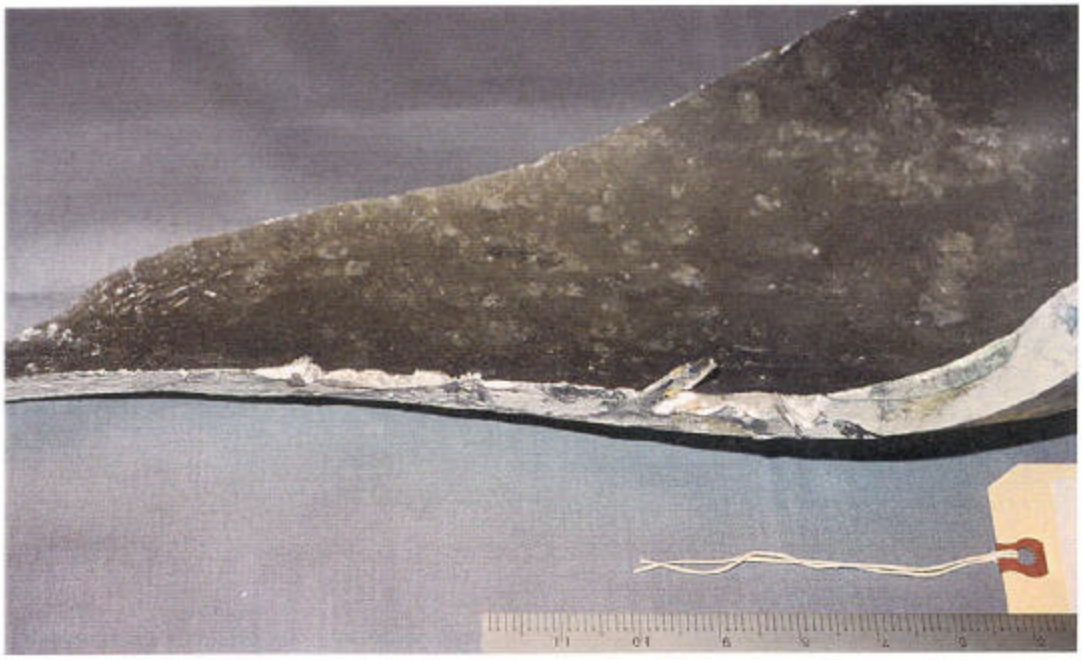

Photo ID: DC18129-R1E23

Photo ID: DC18129-R2E10

Photo ID: DC18129-R2E11

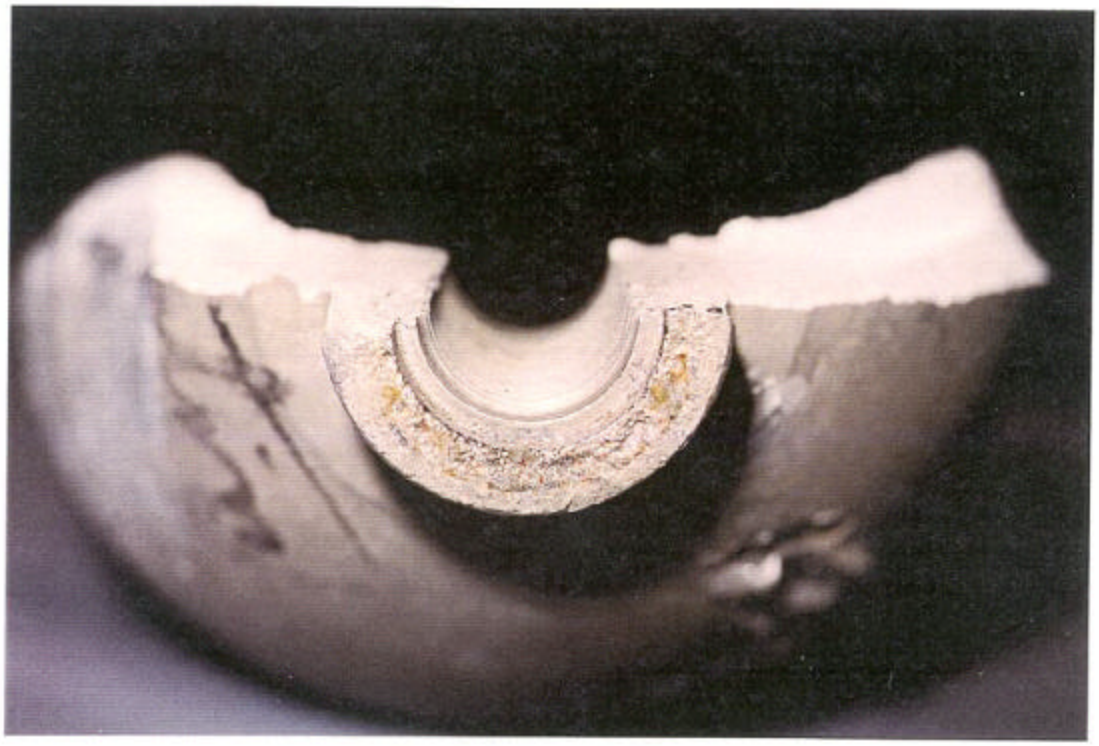

Photo ID: DC18129-R2E6

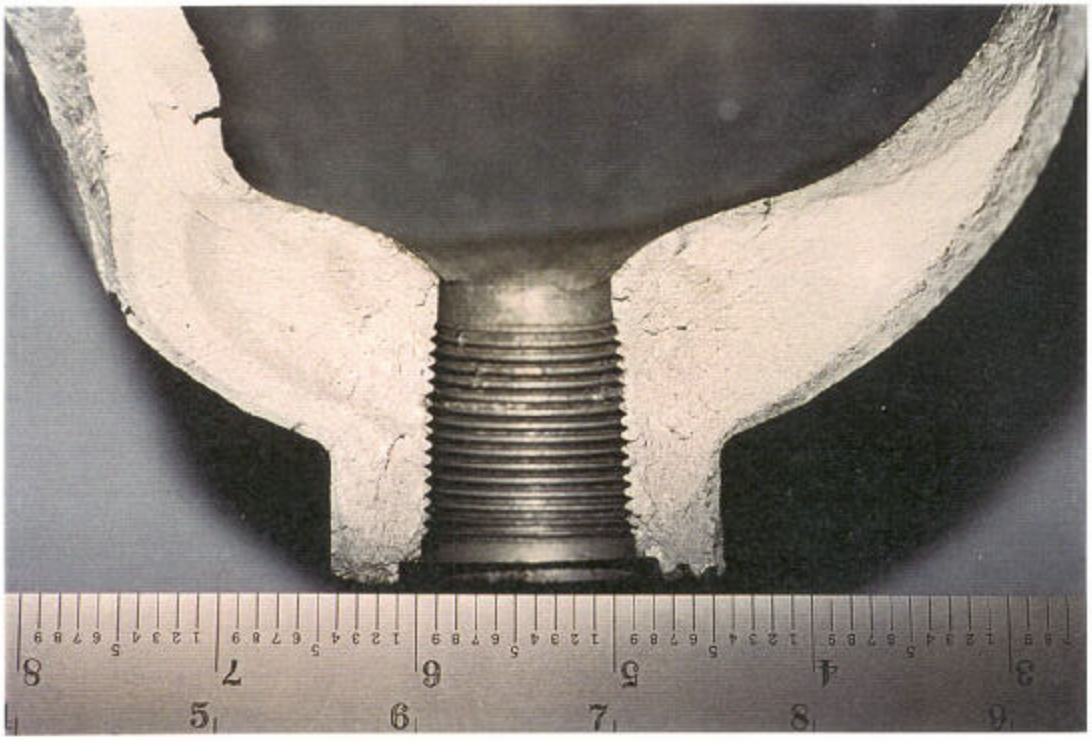

Photo ID: DC18129-R2E7

EX.

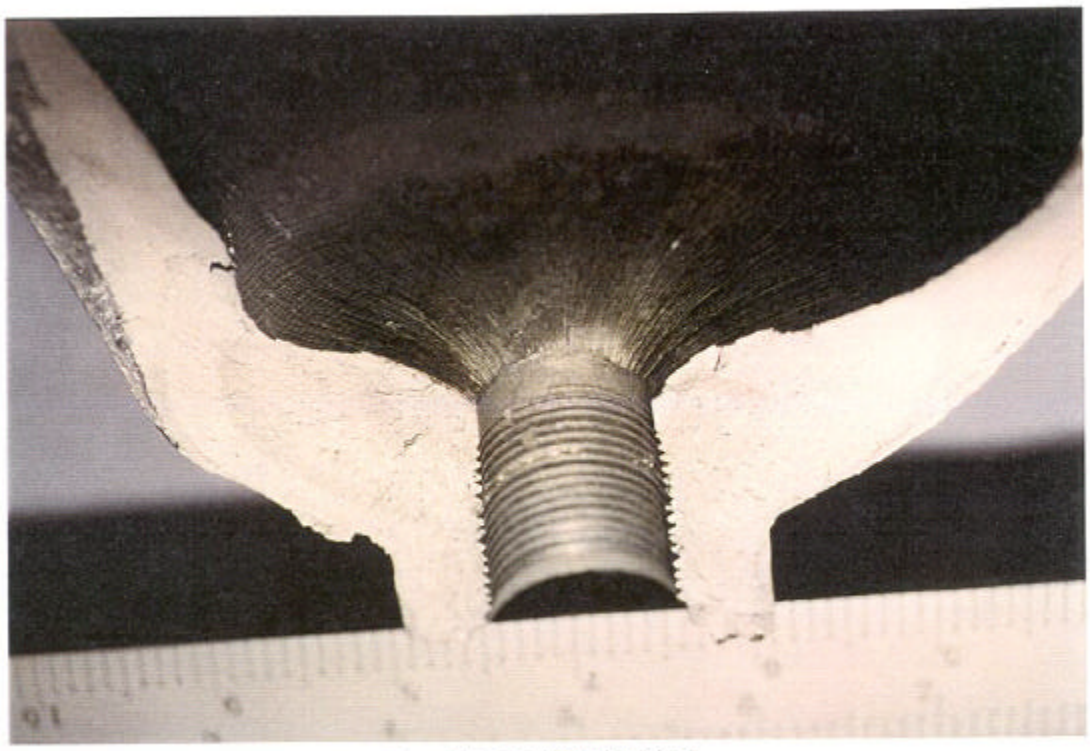

Photo ID: DC18129-R2E8

Photo ID: DC18129-R2E9

Photo ID: DC18129-R2E12

Photo ID: DC18129-R2E16

Ex.

Photo ID: DC18129-R2E13

Photo ID: DC18129-R2E15

Ex.

Photo ID: DC18129-R2E18

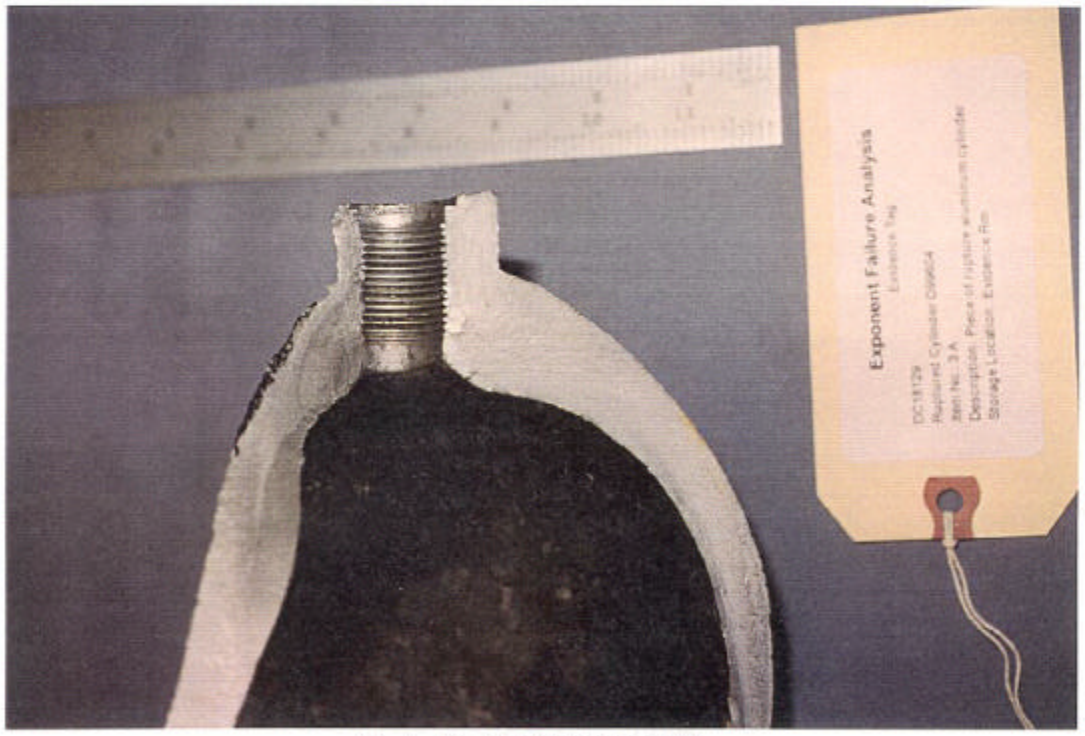

Photo ID: DC18129-R2E19

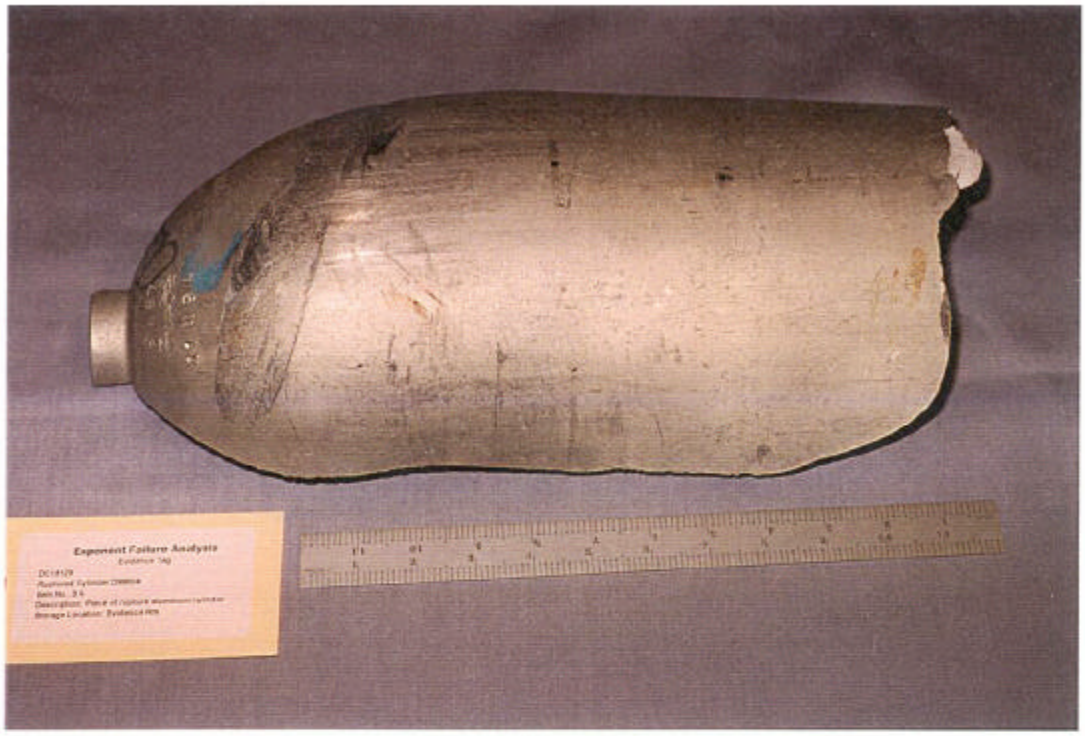

Photo ID: DC18129-R3E2

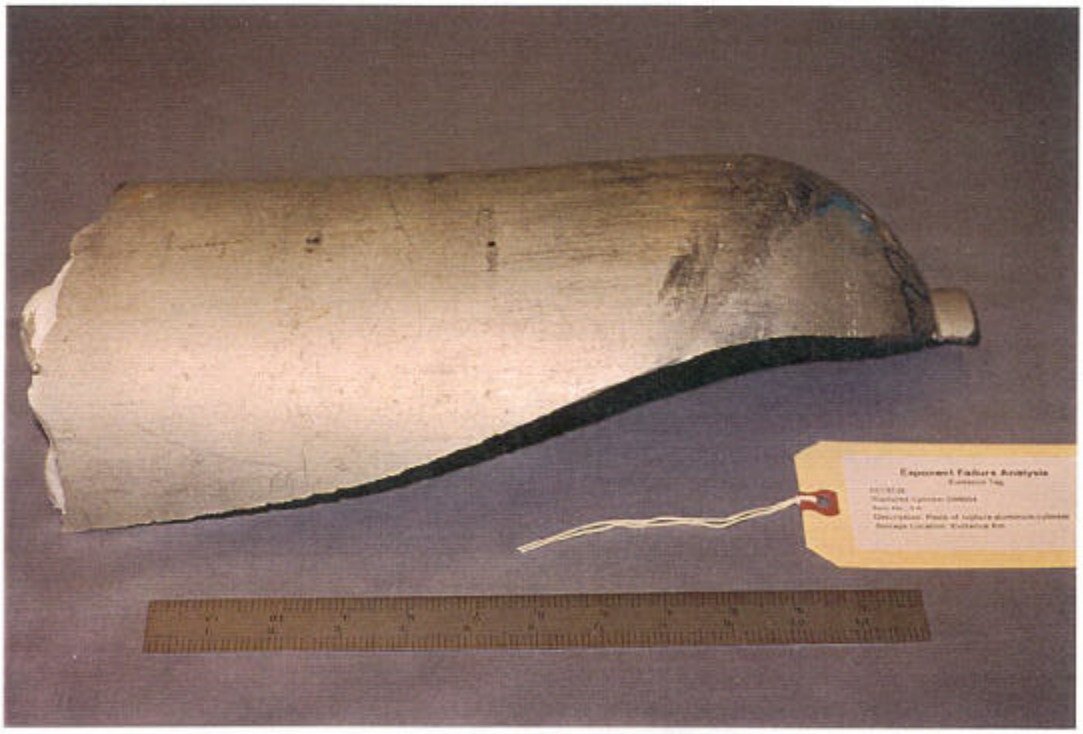

Photo ID: DC18129-R3E7

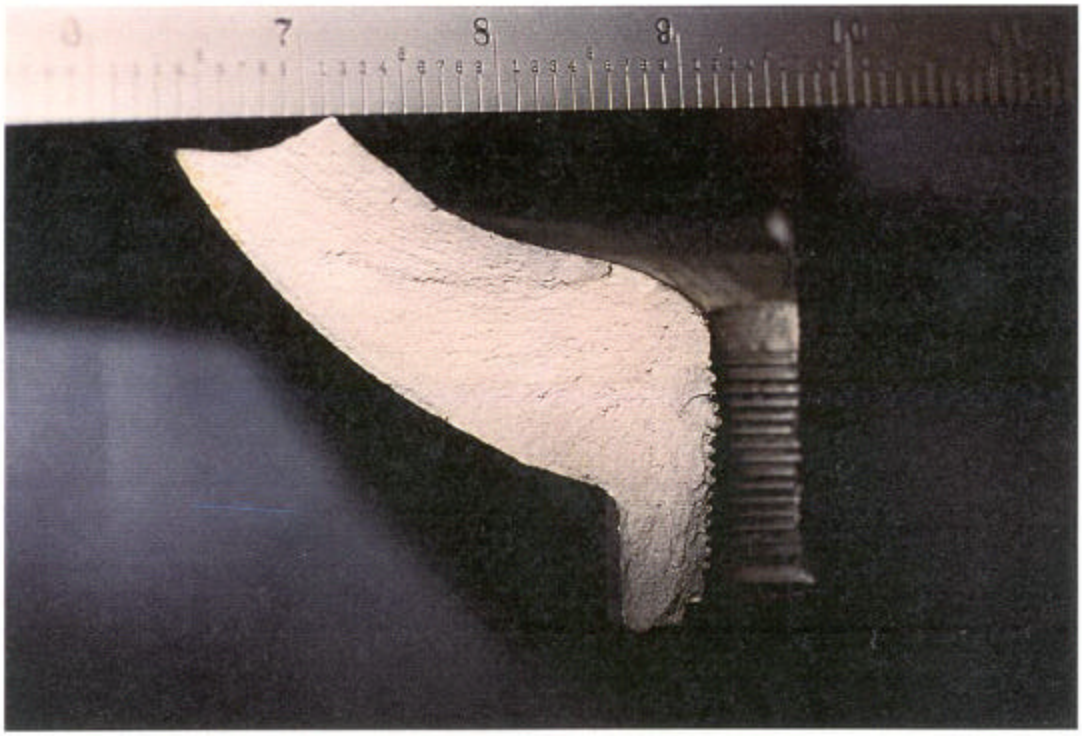

Photo ID: DC18129-R2E22

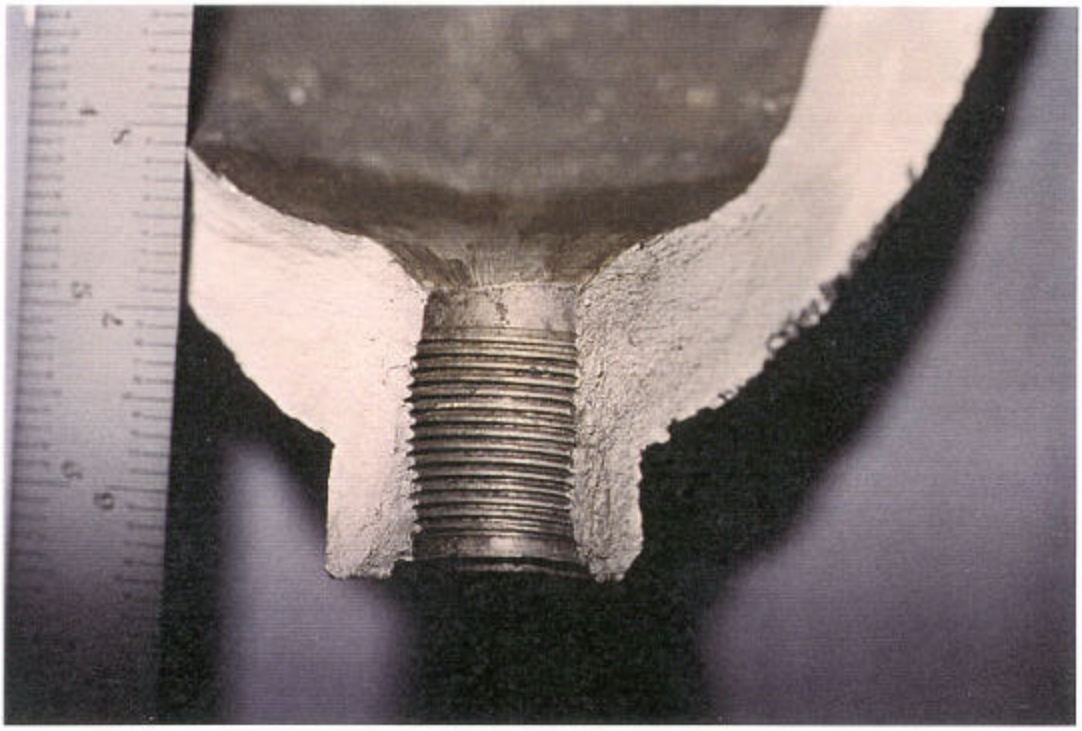

Photo ID: DC18129-R2E23

Ex.

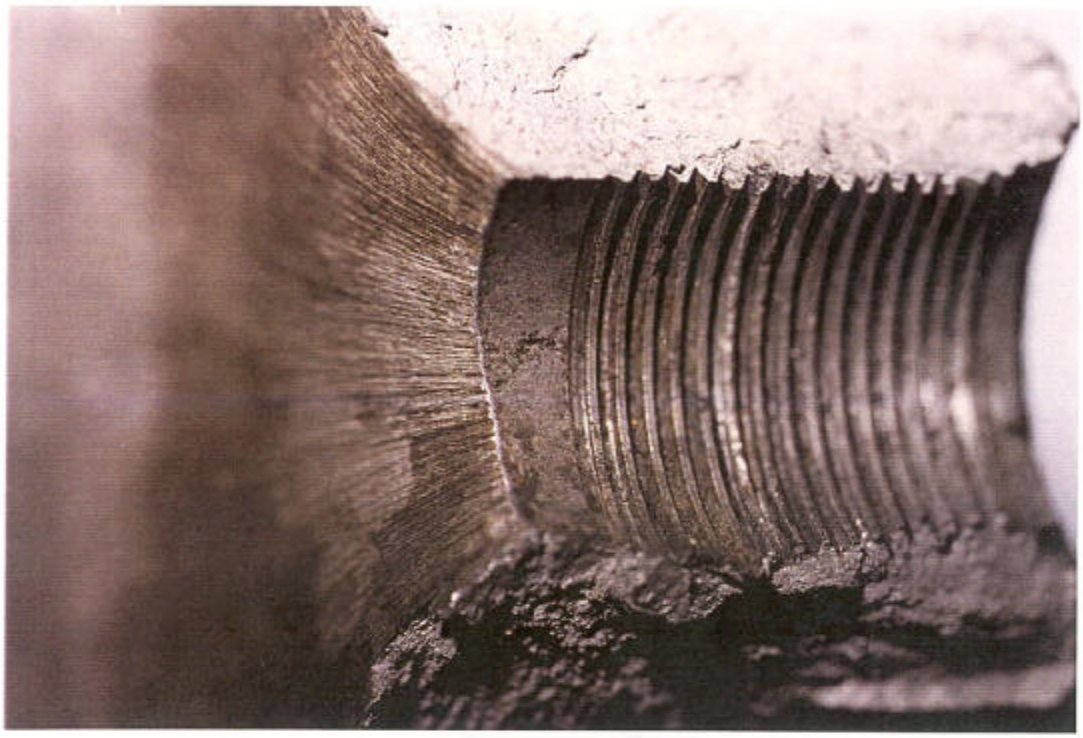

Photo ID: DC18129-R2E24

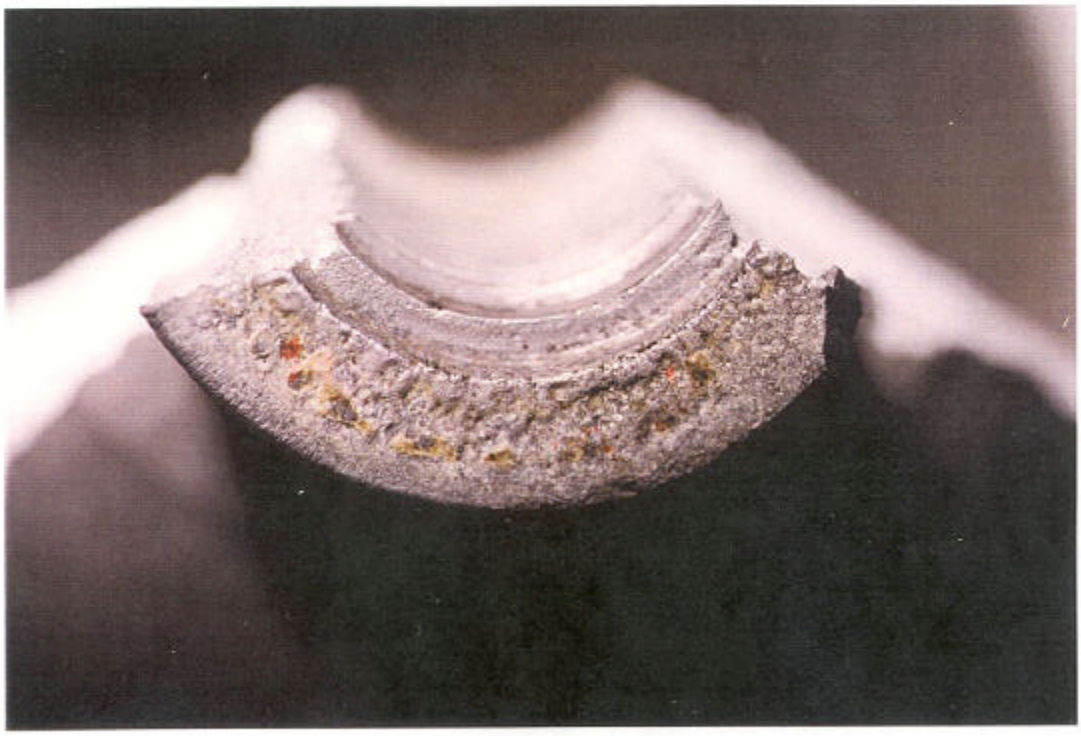

Photo ID: DC18129-R2E25

Ex.

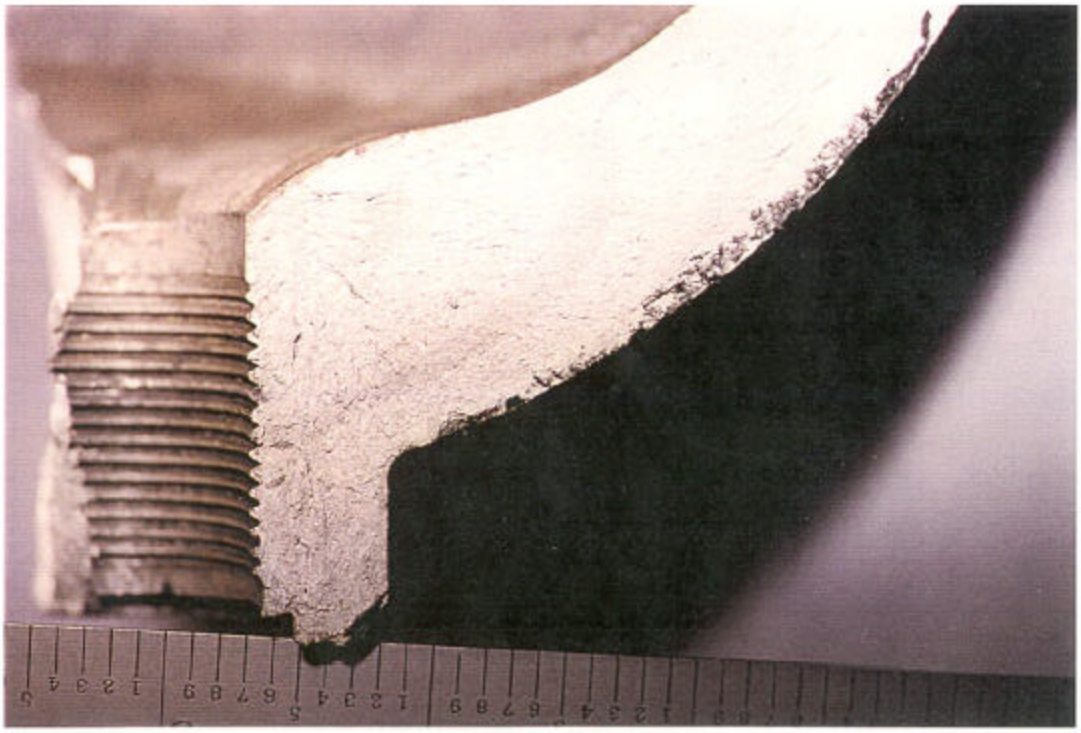

Photo ID: DC18129-R3E8

Photo ID: DC18129-R3E5

Ex.

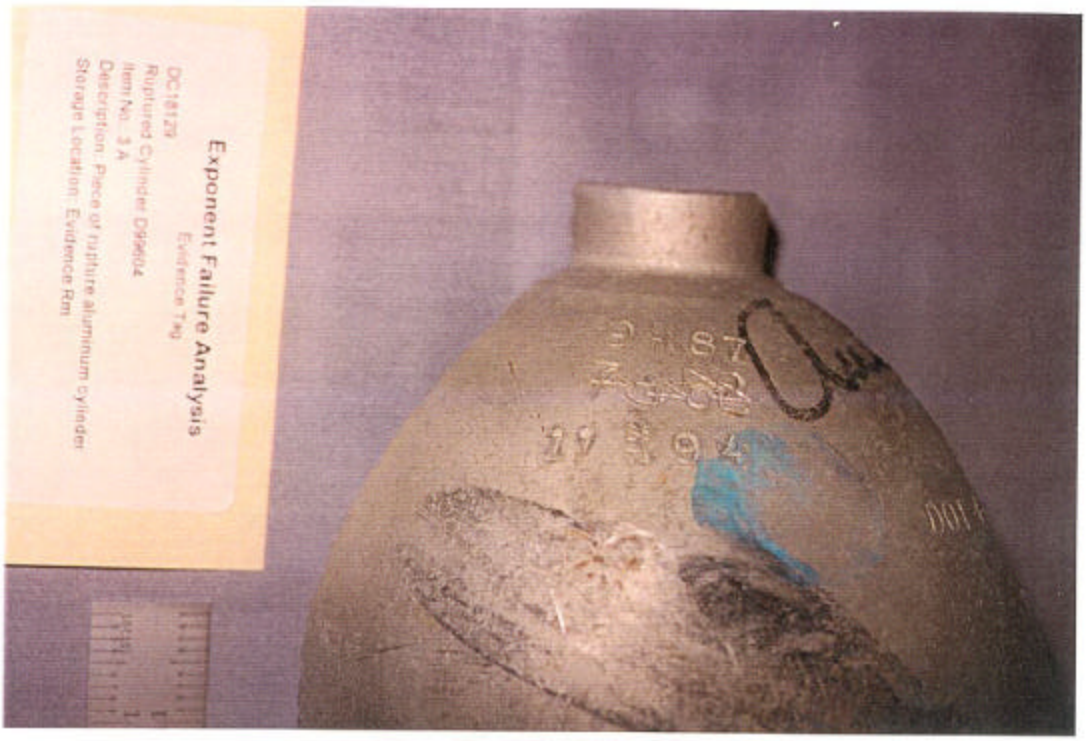

Photo ID: DC18129-R3E3

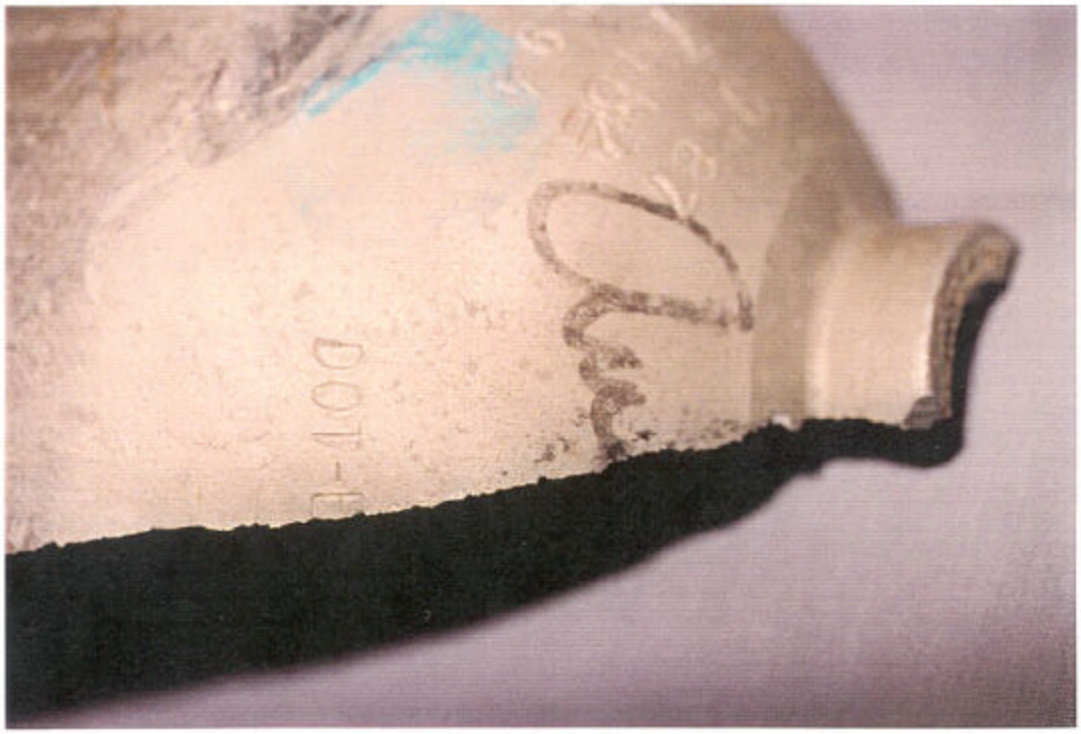

Photo ID: DC18129-R3E4

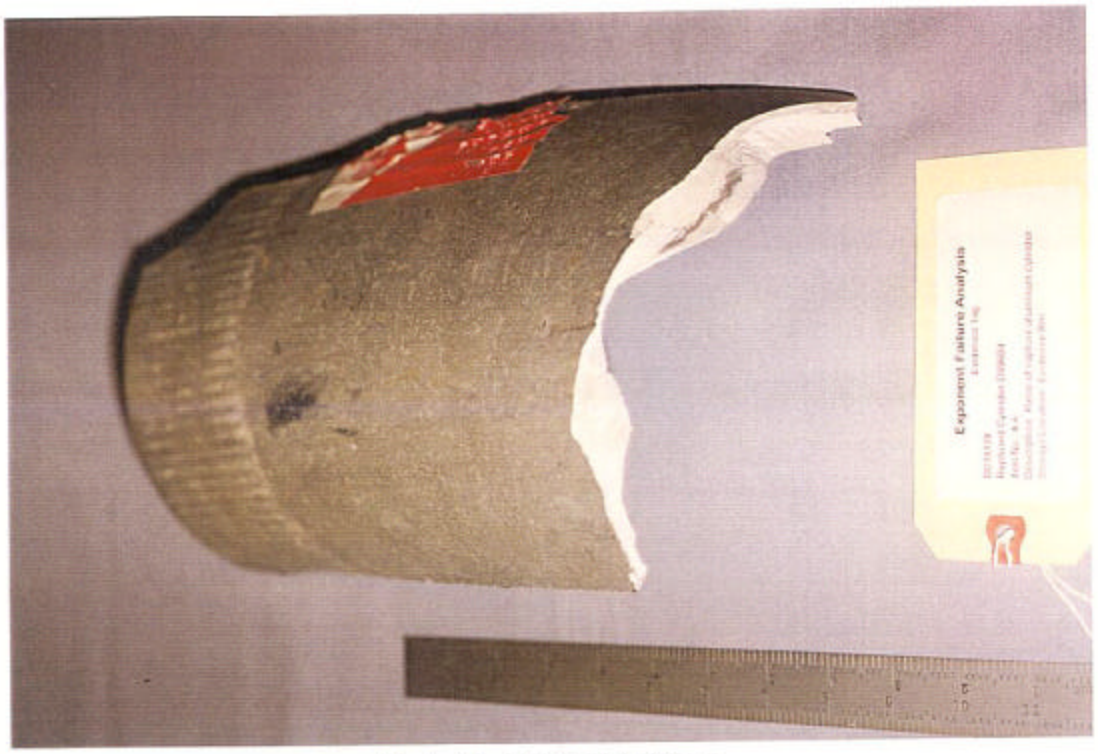

Photo ID: DC18129-R3E14

Photo ID: DC18129-R3E12

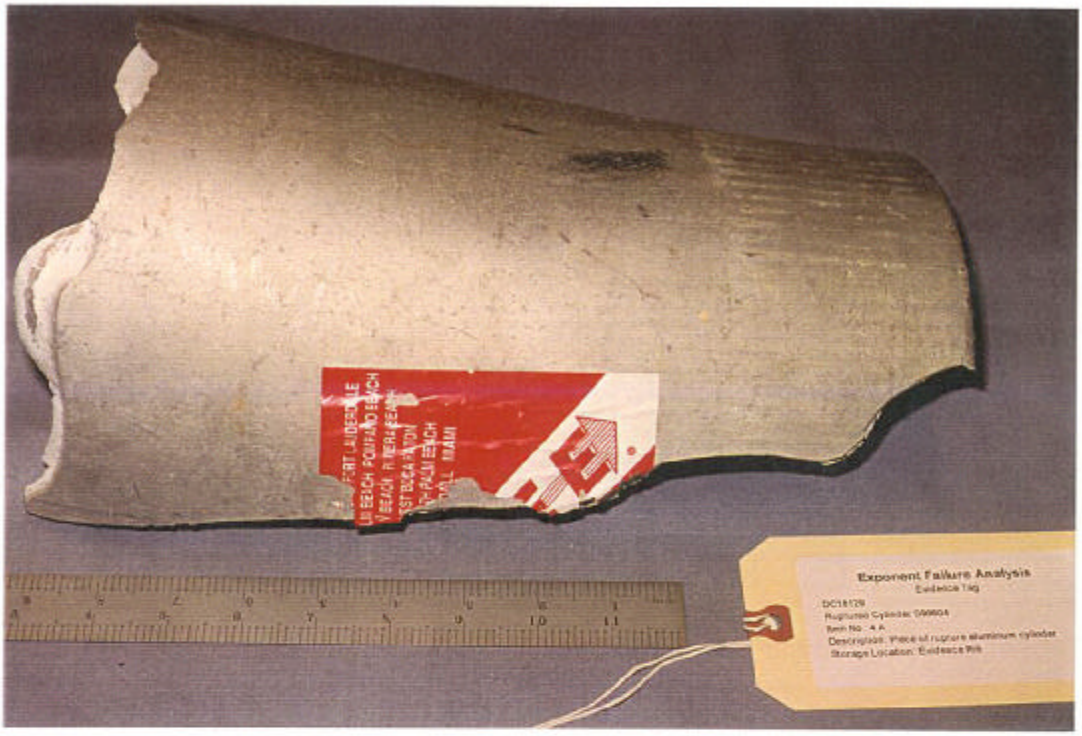

Photo ID: DC18129-R3E15

Photo ID: DC18129-R3E17

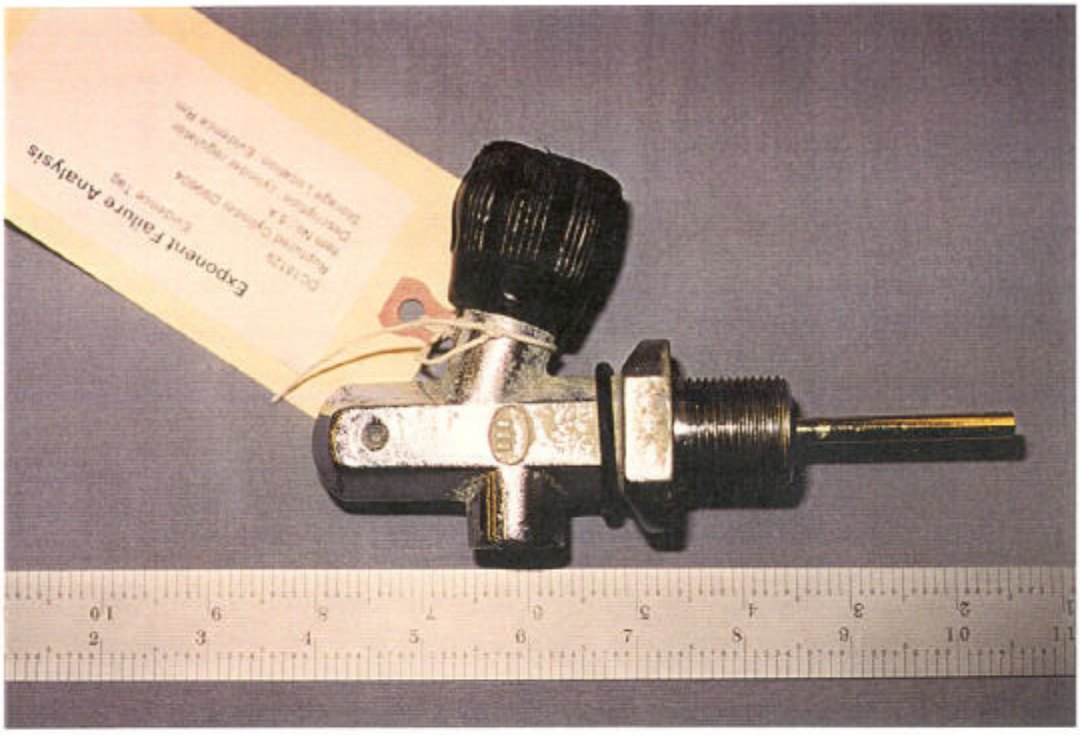

Photo ID: DC18129-R3E20

Photo ID: DC18129-R3E19

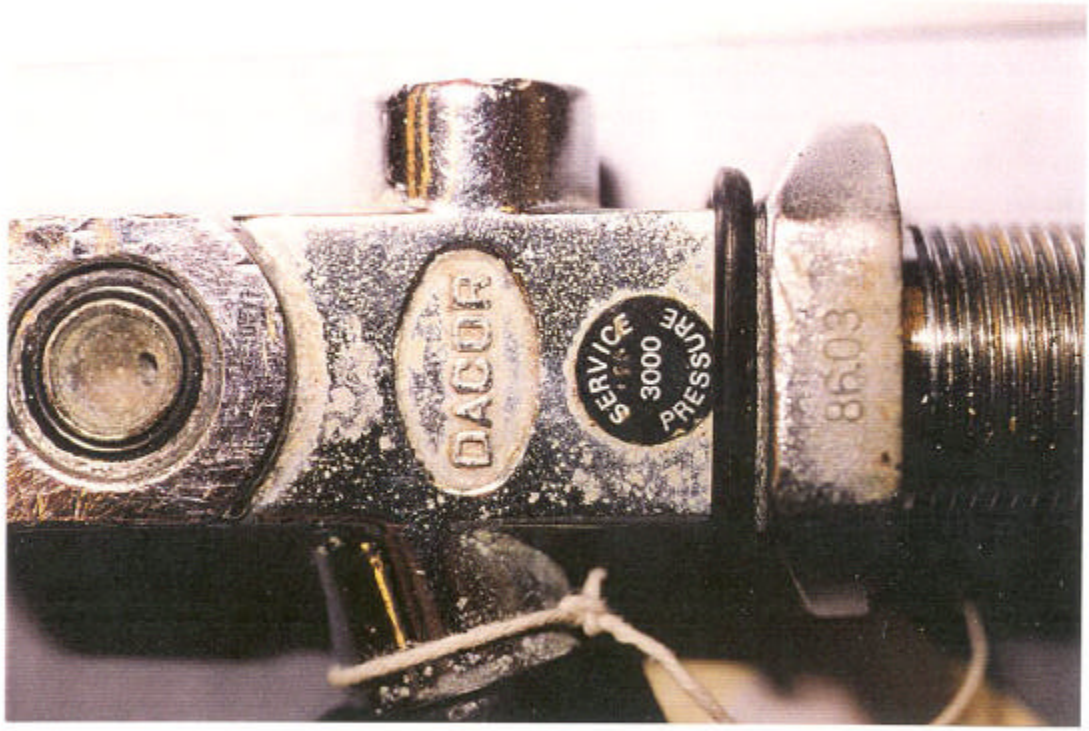

Photo ID: DC18129-R3E24

Photo ID: DC18129-R3E22

Ex.

Photo ID: DC18129-R3E23

Photo ID: DC18129-R3E21